Voltage Regulation for Distribution Networks with Smart Photovoltaic Inverters

Yao Long

A dissertation
submitted in partial fulfillment of the
requirements for the degree of

Doctor of Philosophy

University of Washington

2021

Reading Committee:

Daniel Kirschen, Chair

Baosen Zhang

Brian Johnson

Program Authorized to Offer Degree:
Electrical and Computer Engineering

University of Washington

Abstract

Voltage Regulation for Distribution Networks with Smart Photovoltaic Inverters

Yao Long

Chair of the Supervisory Committee:
Donald W. and Ruth Mary Close Professor Daniel Kirschen
Electrical and Computer Engineering

Traditional mechanical device-based voltage regulation becomes less effective when the high penetration of photovoltaic (PV) generation introduces rapid and frequent voltage fluctuations to the distribution networks. The PV inverters which are able to provide fast and flexible reactive power compensation are thus encouraged to participate in the voltage regulation. Particularly, the smart PV inverters with sensing, communicating and computing capabilities are able to act autonomously and cooperatively. This dissertation studies the coordinated voltage regulation for distribution networks with smart PV inverters. For the coordination among the large number of smart inverters, we develop an adaptive coalition formation-based strategy. This strategy enables the PV inverters to determine their scope of cooperation according to the real-time network operating condition. The PV inverters are thus able to eliminate voltage violations and fairly share the required reactive power contribution according to their maximum available regulation capacity. For the coordination between the smart inverter group and the utility-controlled mechanical devices, we propose a bi-level optimization-based voltage regulation framework. This bi-level optimization model captures the interactions between the different types of devices and allows them to cooperatively optimize their voltage regulation goals. This two-timescale framework ensures global economical efficiency while maintaining satisfactory dynamic regulation performances. Both studies are demonstrated based on realistic distribution networks with field-recorded data.

TABLE OF CONTENTS

LIST OF FIGURES

LIST OF TABLES

GLOSSARY

ADMM: Alternating Direction Method of Multipliers.

ADMS: Advanced Distribution Management System.

CB: Capacitor Bank.

DER: Distributed Energy Resources.

DG: Distributed Generation.

EPRI: Electric Power Research Institute.

IEC: International Electrotechnical Commission.

IEEE: Institute of Electrical and Electronics Engineers.

KKT: Karush-Kuhn-Tucker.

MATPOWER: An open-source tools for electric power system simulation and optimization.

MILP: Mixed Integer Linear Programming.

MISOCP: Mixed Integer Second-Order Cone Programming.

OLTC: On-Load Tap Changer.

PLC: Power Line Communication.

PV: Photovoltaic.

SCADA: Supervisory Control and Data Acquisition.

SOCP: Second-Order Cone Programming.

SVR: Step Voltage Regulator.

TRCA: Toronto and Region Conservation Authority.

VVC: Volt/VAR Control.

ACKNOWLEDGMENTS

Throughout my Ph.D. study, I have received a great amount of help and support from many amazing people. Without them, this work would not have been possible.

First and foremost, I would like to express my sincere gratitude to my advisor Prof. Daniel S. Kirschen, for guiding me through the academic research process, for teaching me how to work with students as a TA, for allowing me to freely choose research and internship projects, for helping me to expand my professional connection, for trusting me when I progress slowly, for encouraging me when I have self-doubt. I was extremely lucky to pursue the doctoral degree under his supervision. All the research skills, communication skills, interpersonal skills I learned from him would be invaluable for my future career and life.

I would like to thank my reading committee member, Prof. Baosen Zhang and Prof. Brian Johnson, for their insightful feedback and suggestions for my research. I am also grateful to Prof. Brandi M. Cossairt for serving as the graduate school representative, Prof. Richard Christie and Prof. Linda Bushnell, for serving in my qualifying exam committee, Prof. Radha Poovendran, for guiding me in my first year. In addition, I extend my thanks to the Clean Energy Institute for funding my research through their fellowship program. I would like to thank all the faculty and staff members that have added to my experiences during my research and study at the University of Washington.

I was fortunate to have two wonderful internship experiences. I would like to thank Prashant Kansal, Sarah Walinga, Akbo Rupasinghe and Hussam Alatrash from Tesla. I have really enjoyed working with them to accelerate the world's transition to sustainable energy. I would like to thank Fang Guo and Jun Du from Morgan Stanley, for introducing me to the quantitative finance industry, for teaching me the professional skills for this industry, and

for providing helpful career advice. I am also grateful to everyone I met in Morgan Stanley, they turned this virtual internship into a rewarding one.

I have had a great pleasure working with many smart and talented people at the University of Washington. A special thank you to Ryan Elliott, for teaching me all the details about how to write a research paper and for being a patient, meticulous and trustworthy collaborator. A big thank you to Yuanyuan Shi, Atinuke Ademola-Idowu, Yize Chen, Yushi Tan, Hao Wang, Zeyu Wang, Yishen Wang, Ting Qiu, Bolun Xu, Pan Li, Abeer Almaimouni, Daniel Olsen, for the useful exam preparation advice and for the important tips about how to survive the Ph.D. program. I would like to thank Xuhang Ying, Zhipeng Liu, Baicen Xiao, Sang Sagong, Qiong Lin, Phillip Lee, Andrew Clark for helping me settle into the Ph.D. program. I also would like to recognize the assistance and support I received from: Mareldi Ahumada, Wenqi Cui, Ling Zhang, Chanaka Keerthisinghe, Yue Sun, Nam Song, Trisha Ray, Daniel Tabas, Nina Vincent, Lane Smith, Rahul Mallik, Soham Dutta, Minghui Lu, Chenghui Tang, Yaohua Cheng, Qingchun Hou, Hao Li.

I also wish to thank my friends. To Yiming, for always being able to get my jokes. To Xiujin, for being the first person in Seattle to welcome me. To Shiyao, for the lunch time and movie time. To Rong, for the long walks and long chats around Green Lake. To Xun, Yuyang and Fangyi, for being the best roommate. To Yaxuan, Chen, Weisi, Fan, Xiasen, Ming and Yang for the hotpot, fried chicken, barbecue, board games and Karaoke. To my guitar and eReader, for accompanying me whenever I need some distraction.

Lastly, and most importantly, I would like to thank my family. A special thanks to my uncle Zhigang and aunt Xianghui, for always encouraging and supporting me to dream big. A huge thanks to my little sister Fan, for being my major emotional support and for always reminding me what's really important in life. My deepest gratitude to my parents, Hongping and Zhihua, for their unconditional and unparalleled love, support and encouragement over the years, and also for the fantastic recipes and the incredibly useful household tips.

DEDICATION

to my parents and sister

Chapter 1

INTRODUCTION

1.1 Voltage regulation in distribution networks

Keeping the network voltage within a satisfactory range plays a vital role in maintaining the performance of the distribution networks and the quality of the power delivered. In a traditional distribution network, voltage magnitude typically decreases from the substation to the end of the distribution feeder. To compensate for such line drops, voltage regulation usually employs the on-load tap-changing (OLTC) transformer or step voltage regulators (SVR) to raise their downstream voltage, or the capacitor banks (CBs) to boost the local voltage level [1]. However, in recent years, the distribution networks have been experiencing a rapid increase of the distributed generation (DG), particularly the small-scale photovoltaic (PV) generation. For example, Fig. 1.1 shows the increase of the small-scale solar capacity in eight states of the United States. With 1.5 gigawatts (GW) added in 2020, the total installation capacity of California reaches 10.6 GW as of December 2020. Together with the environmental benefits, new voltage regulation challenges have also been brought into the distribution networks with the proliferation of PV generation[2, 3].

Traditionally, the power flows in a single direction, i.e., from the transmission grid to the load. However, in a distribution network with high penetration of small-scale PV generation. Reverse power flow would occur when the PV generation exceeds the local load. As the distribution lines generally have a high impedance and low X/R ratio, the reverse power flow can cause a increased terminal voltage which might even exceed the upper voltage limit [4]. In addition, the PV generation is highly variable due to the intermittency in the solar irradiance. Such rapid variations in PV active output would induce fast voltage fluctuations in the distribution networks [5]. Traditional mechanical voltage regulation devices are less

effective in handling these voltage fluctuations. Moreover, such fluctuations may trigger the frequent operation of these voltage regulation devices, which lead to their increased mechanical wear-and-tear [6, 7]. Another voltage regulation challenge arises as the small-scale PV generations are usually randomly scattered in the distribution networks [8]. The uneven distribution of PV generation capacity would result in different impacts to the voltage across the geographical zones [9]. The large voltage differences exist in a distribution network can become problematic for the voltage regulation with OLTC [10]. To deal with these issues, new voltage regulation devices and methods are needed in the distribution networks.

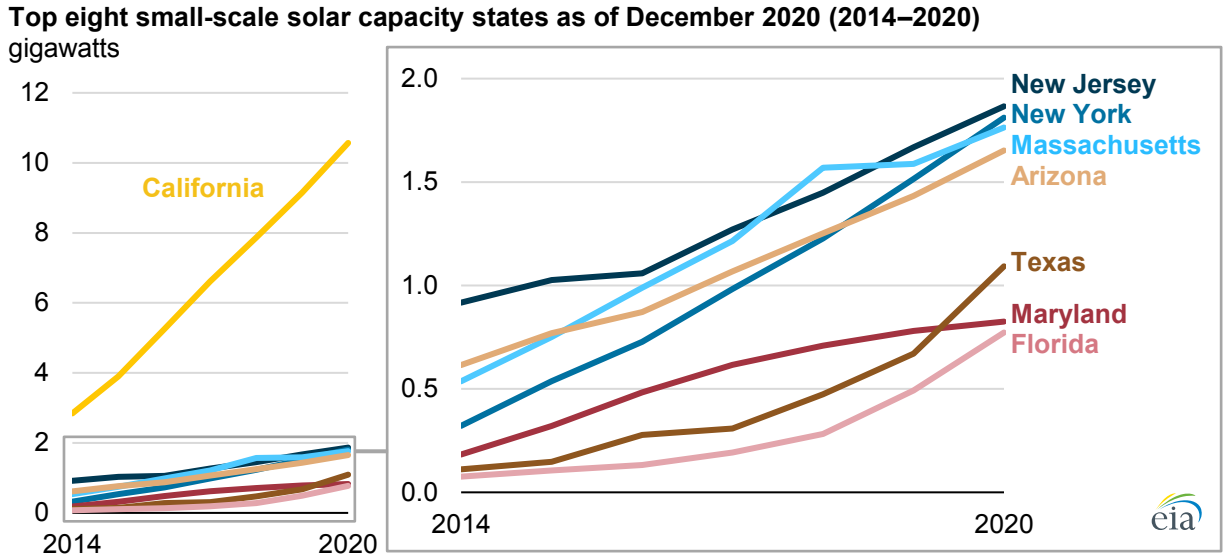

Figure 1.1: Source: U.S. Energy Information Administration, based on states' small-scale solar PV capacity. https://www.eia.gov/todayinenergy/detail.php?id=46996.

1.2 Voltage regulation with smart PV inverters

The integration of PV generation also introduces a new voltage regulation device to the distribution network - the smart PV inverter. The smart PV inverters are generally equipped with measuring, computing and communicating capabilities [11, 12]. They are thus able to provide advanced and autonomous control functions beyond the basic power conversion and

energy feeding functions [13]. The participation of the smart inverters in voltage regulation has been advocated by grid codes like IEEE standard 1547 and CA Rule 21. Their volt-var function is also defined as one of the smart inverter's common functions by worldwide stakeholders in the industry collaborative initiative facilitated by EPRI [14]. Currently, the PV inverters provides reactive power compensation mainly according to their local voltages based on piece wise-linear functions. While with the development in information and communication technology, as well as the establishment of distributed energy resource (DER) interconnection and interoperability standards, a more coordinated voltage regulation architecture for the distribution network would become possible.

To accommodate the smart PV inverters, voltage regulation in distribution networks generally facilitates the coordination on two timescales. The faster timescale coordination just involves the large number of smart inverters that are distributed across the distribution networks. These smart inverters are able to act autonomously according to the real-time network operating condition. They are also able to act cooperatively by using communication tools like Wi-Fi, ZigBee or power line communication (PLC). Due to their fast and flexible operation, the smart inverters are usually applied to eliminate the real-time network voltage violations caused by the variability in load or PV active generation. Ideal coordination strategies for these devices need to be able to quickly adapt to the network operating condition, reliably function under communication problems, flexibly support their plug-and-play operation, etc. On the other hand, traditional mechanical voltage regulation devices like OLTC and CBs operate on a much slower timescale. They are also less flexible in the regulation actions. However, these devices typically have a larger impact on the network voltage level and the reactive power flow. Their setpoints are thus usually optimized and dispatched by the system operator based on a full knowledge of the network to improve the economical performance of the entire distribution network. To ensure the optimal schedule of these mechanical devices in the presence of a large group of cooperative smart PV inverters, a proper way to model the interactions between these two types of devices and thus to coordinate their regulation actions are necessary.

1.3 Scope and outline of the work

This thesis is organized as follows:

- *Chapter 1: Introduction* presents research background and motivation.

- *Chapter 2: Adaptive Coalition Formation-Based Coordinated Voltage Regulation in Distribution Networks* addresses the coordination among the smart PV inverters. Section 2.3 proposes a coalition formation scheme for the PV inverters to determine their scope of cooperation. Section 2.4 develops a distributed strategy to coordinate the control actions within each voltage regulation coalition.

- *Chapter 3: Bi-level Volt/VAR Optimization in Distribution Networks with Smart PV Inverters* focuses on the coordination among all the voltage regulation devices. 3.2 presents a bi-level optimization model to capture the interactions between the smart inverter group and the utility-controlled mechanical device. 3.3 proposes the solution approach and the corresponding two-timescale voltage regulation framework.

- *Chapter 4: Conclusion* concludes the thesis and provides suggestions for future work.

Chapter 2

ADAPTIVE COALITION FORMATION-BASED COORDINATED VOLTAGE REGULATION IN DISTRIBUTION NETWORKS

High penetrations of photovoltaic (PV) systems can cause severe voltage quality problems in distribution networks. This chapter proposes a distributed control strategy based on the dynamic formation of coalitions to coordinate a large number of PV inverters for voltage regulation. In this strategy, a rule-based coalition formation scheme deals with the zonal voltage difference caused by the uneven integration of PV capacity. Under this scheme, PV inverters form into separate voltage regulation coalitions autonomously according to local, neighbor as well as coalition voltage magnitude and regulation capacity information. To coordinate control within each coalition, we develop a feedback-based leader-follower consensus algorithm which eliminates the voltage violations caused by the fast fluctuations of load and PV generation. This algorithm allocates the required reactive power contribution among the PV inverters according to their maximum available capacity to promote an effective and fair use of the overall voltage regulation capacity. Case studies based on realistic distribution networks and field-recorded data validate the effectiveness of the proposed control strategy. Moreover, comparison with a centralized network decomposition-based scheme shows the flexibility of coalition formation in organizing the distributed PV inverters. The robustness and generalizability of the proposed strategy are also demonstrated.

2.1 Introduction

Installations of rooftop photovoltaic (PV) systems are growing rapidly. In 2019, around 42 GW of rooftop PV systems were installed worldwide and SolarPower Europe estimated that the global installed capacity will rise to 65 GW by 2024 [15]. Because they have a much larger R/X ratio than transmission networks, voltages in distribution networks are quite sensitive to the active power generated by distributed PV systems. Distribution networks with a high penetration of PV are therefore likely to experience several voltage quality problems[16, 17, 10]:

- Over-voltages when the PV generation exceeds the local load and the power flow reverses;
- Rapid voltage fluctuations caused by sudden changes in solar irradiance;
- Large voltage differences between nodes due to the uneven distribution of PV generation capacity.

Traditional voltage regulation relies on devices such as step voltage regulators (SVR), on-load tap-changing (OLTC) transformers, and capacitor banks (CB). However, these devices are intended to manage voltage variations on a time-scale of hours, and they are not able to deal with the rapid fluctuations in the output of PV systems [6, 7]. On the other hand, PV inverters are capable of providing fast and flexible reactive power compensation. IEEE standard 1547 standard encourages their contribution to voltage regulation [18].

2.1.1 Literature Review

Existing voltage regulation architectures can be broadly classified into three categories. Control schemes of the first category, such as the droop-based Volt/VAR control (VVC) [19], rely solely on local measurements. Because they lack a global perspective and coordination, these controllers may not deploy the available resources effectively. The second category

involves a centralized architecture, where a central controller with full knowledge of the network dispatches all controllable devices [20]. While theoretically optimal, such an approach requires extensive communications and involves complex computations. Moreover, it makes the system susceptible to a single point of failure. Distributed control architectures make up the third category. In this approach, individual controllers cooperate using communications with a limited number of neighbors to achieve a common goal. The computation and communication burden are allocated to individual controllers, which makes this approach more robust to communication failures and better able to coordinate the control of distributed voltage regulation devices in real-time.

Several authors have approached distributed voltage control as an optimization problem and implemented algorithms such as dual-ascent [21], primal-dual gradient [22] to solve it in a distributed manner. Though these optimization-based control strategies provide convergence and optimality guarantees under assumptions of power flow linearity and static power consumption, they usually require knowledge of the exact values of the system parameters, such as line impedance, which are not always available for distribution networks. Several model-free control strategies have also been proposed to coordinate local droop-controlled voltage regulation devices, among them strategies based on consensus algorithms. Using peer-to-peer communication, these strategies aim to allocate the required control actions, e.g. reactive power compensation or active power curtailment, fairly among PV inverters based on their available capacity [23, 24, 25, 26, 27, 28]. In [23, 24, 25], a leader inverter measures its local voltage and updates its utilization ratio, which is the ratio of the inverter's power output used for voltage regulation to its maximum available power capacity. This ratio is delivered to all the follower inverters via neighboring communication according to the leader-follower consensus algorithm. Every follower inverter accepts this utilization ratio and adjusts its power output accordingly. After the leader inverter stops updating and the utilization ratio has been fully communicated, every participating inverter shares an equal utilization ratio. Some authors [23, 24] make the assumption that the highest or lowest voltage always occurs at the end node of the radial feeder and choose the inverter at

this node to be the leader. However, this assumption does not always hold true when PV capacity is unevenly distributed along the feeder. Zeraati et al. [25] extended this approach to let any PV inverter that can experience a voltage limit violation act as the leader. The need to appoint a leader is relaxed in [26, 27, 28]. In those control strategies, each inverter measures the local voltage and determines its own utilization ratio. This ratio is gradually adjusted based on the consensus algorithm to reflect its neighbors' contribution to voltage regulation.

2.1.2 Contribution

This chapter considers the same voltage regulation objectives as in [23, 24, 25, 26], i.e. maintaining the voltage magnitude within a satisfactory range and equalizing the utilization ratio of the participating inverters. These two objectives can conflict because equalizing the utilization ratio means that voltage violations are eliminated by increasing or decreasing the voltage across the entire network. However, if the PV generation capacity and the load are distributed unevenly, simultaneous upper and lower voltage limit violations can occur on a feeder. In this case, requiring an equal utilization ratio would either solve the over-voltage problem at certain nodes at the expense of making the under-voltage problem at other nodes even worse, or vice-versa. Therefore, a system-wide consensus on the utilization ratio becomes detrimental. To fairly share the voltage regulation burden among PV inverters while satisfying the voltage constraints, one must be able to distinguish between situations where reaching a system-wide consensus is desirable and situations where the inverters should reach a localized consensus about an equal utilization ratio. In multi-agent control, a coalition refers to a goal-directed and short-lived group formed by the smart agents to complete a common task cooperatively[29]. PV inverters equipped with sensing, communicating and computing capabilities can be treated as smart agents who can work together at regulating voltages [11, 12]. These smart PV inverters could be empowered to form coalitions that can reach an effective consensus about what needs to be done to regulate voltages.

This chapter proposes a distributed scheme where PV inverters organize themselves into

different voltage regulation coalitions using local decision-making based on voltage magnitude as well as regulation capacity information. Within each coalition, a feedback-based leader-follower consensus algorithm determines the utilization ratio of each inverter. The main contributions of this chapter are:

- An adaptive coalition formation scheme which effectively solves potential conflicts between voltage regulation and reactive power sharing. In this scheme, PV inverters use a simple and clear decision logic to determine the scope of their cooperation. They can therefore organize themselves efficiently and flexibly to adapt to constantly varying network operating condition.

- An improved leader-follower consensus algorithm which effectively eliminates voltage violations and equalizes the utilization ratios in each coalition. Instead of relying on a fixed leader, this algorithm enables each PV inverter to adaptively determine whether it is a leader or a follower based on its voltage deviation. The connection with the distributed optimization algorithm demonstrates the theoretical foundation of this algorithm.

- A model-free two-timescale distributed control strategy which fully exploits the autonomous capability of the smart PV inverters to regulate voltages. This strategy enables each inverter to act in response to real-time network conditions, and does not require central control or prior knowledge of the network. Hence, it is not only able to adapt to changing network conditions and configurations, but can also scale to accommodate an arbitrary number of inverters. We demonstrate the robustness and generalizability of the proposed strategy using simulation-based case studies.

2.1.3 Chapter Organization

The remainder of this chapter is organized as follows. Section 2.2 introduces the overall control framework. Sections 2.3 and 2.4 describe the details of the voltage regulation coalition

formation scheme and the within-coalition coordination. Section 2.5 discusses the implementation issues. Section 2.6 and 2.7 present and analyze simulation results. Section 2.8 concludes.

2.2 Overview of the Proposed Control Strategy

2.2.1 Communication Network

In this chapter, we treat the distribution network as a cyber-physical system, where each PV inverter is able to:

- Acquire local measurements;
- Communicate with its neighbors;
- Compute necessary control actions;
- Execute these control actions.

Communication within a network of n PV inverters can be represented by a directed graph $\mathcal{G} = (\mathcal{V}, \mathcal{E})$, where $\mathcal{V} = \{1, 2, ..., n\}$ is the set of nodes and $\mathcal{E} \subseteq \mathcal{V} \times \mathcal{V}$ is the set of edges. Each node corresponds to a PV inverter and $(i, j) \in \mathcal{E}$ if inverter i can receive information from inverter j. The graph is *connected* if for every pair of nodes there is a path connecting them. The graph is *undirected* if $(i, j) \in \mathcal{E}$ implies $(j, i) \in \mathcal{E}$. The set of neighbors of inverter i is denoted by $\mathcal{N}_i = \{j \in \mathcal{V} : (i, j) \in \mathcal{E}\}$. We define the neighbor set $\mathcal{N}_i$ of inverter i as the collection of inverters that are directly connected to it through power lines without passing other inverters. Specifically, if two inverters are installed on different laterals, they are neighbors if they do not have a common upstream inverter. For example, one could assume that the inverters communicate with their neighbors using Power Line Communication (PLC) [30]. Therefore, the communication network for a typical distribution network is a connected and undirected graph with a tree topology.

2.2.2 Control Objective

The first control objective is to maintain the voltages within the regulation range based on the grid code:

$$\underline{V} \leq V_i \leq \bar{V} \tag{2.1}$$

where V_i is the voltage magnitude of node i, $\underline{V}$ and $\bar{V}$ are the lower and upper voltage limits.

To prevent the excessive use and early saturation of the voltage regulation devices at certain nodes, several authors [23, 24, 25, 26] argue that all devices should operate at the same utilization ratio after reaching equilibrium. However, voltages in some parts of a distribution feeder may exceed the upper limit while voltages in other parts may be below the lower limit. To address this problem, we develop a scheme that allows the PV inverters to self-organize into coalitions. Within each coalition, all inverters operate at the same utilization ratio:

$$\frac{Q_i}{Q_i^{\max}} = \frac{Q_j}{Q_j^{\max}} = u_a,\ \forall i, j \in \mathcal{G}_a \tag{2.2}$$

where u_a is the utilization ratio of coalition $\mathcal{G}_a = (\mathcal{V}_a, \mathcal{E}_a)$, $\mathcal{V}_a \subseteq \mathcal{V}$ and $\mathcal{E}_a \subseteq \mathcal{E}$. Q_i and $Q_i^{\max}$ are the required reactive power contribution for voltage regulation and the maximum available reactive power capacity of PV inverter i.

2.2.3 Control Framework

Fig. 2.1 illustrates the two time-scale voltage regulation strategy. Due to the uneven distribution of load and PV generation capacity, their regular daily variations can lead to large zonal voltage differences at certain times. On the slower time-scale, e.g. every 5 minutes, the coalition formation scheme guides PV inverters to form into separate groups to solve the over-voltage and under-voltage problems that may arise simultaneously in different parts of the network. On the faster time-scale (i.e., the inverter sampling period of tens to hundreds of milliseconds [23, 24, 25, 26, 27, 28]), the feedback-based leader-follower consensus algorithm eliminates the real-time voltage violations and distributes the voltage regulation burden fairly to every inverter within each coalition. Throughout the process, PV inverters

make control decisions based on simple calculations and only need to exchange information with a limited number of neighbors. This control strategy is thus able to coordinate the PV inverters in real-time. Moreover, since there is no need for system information such as line impedance, network topology or nodal upstream-downstream relation, this control strategy can adapt to changes in the network topology and supports a flexible plug-and-play operation of the inverters.

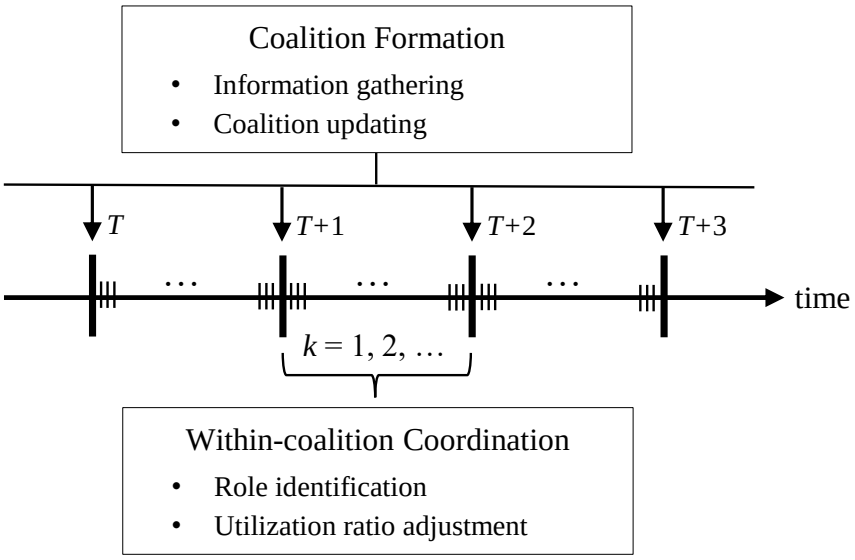

Figure 2.1: Framework of the proposed control strategy.

2.3 Coalition Formation

Upon initialization, the coalition formation scheme starts with a single coalition consisting of every PV inverter. It then periodically alters the set of coalitions to:

- Separate the over- and under-voltage violations and assign them to different coalitions to prevent conflicts between PV inverters;

- Allocate sufficient voltage regulation capacity to each coalition;

- Maintain the connectivity of the communication network within each coalition.

Each time the coalitions are updated, the PV inverters first gather necessary data. Based on this information, they evaluate the current coalition status and determine their actions.

2.3.1 Information Gathering

Before updating the coalitions, each inverter i, $i \in \mathcal{G}_a$ needs to gather the following data:

- Local data: the local voltage magnitude V_i and utilization ratio u_i;
- Neighbor data: the voltage magnitude V_j and utilization ratio u_j of neighbors j, $\forall j \in \mathcal{N}_i$;
- Coalition data: the assessed coalition maximum voltage $V_i^{\max}$ and minimum voltage $V_i^{\min}$ of $\mathcal{G}_a$.

Algorithm 1 shows how inverters obtain the coalition data through neighboring communication. Each inverter measures its local voltage V_i and uses it to initialize its estimate of the coalition maximum voltage $V_i^{\max}$ and minimum voltage $V_i^{\min}$. At each iteration within the time window $[T - \Delta T,\, T]$, the inverter communicates with its neighbors within the same coalition to exchange their estimates. As the iterations progress $V_i^{\max}$ and $V_i^{\min}$ are updated based on the max and min-consensus algorithm. Since the communication network is connected, in a coalition with $|\mathcal{V}_a|$ inverters, after a maximum $|\mathcal{V}_a| - 1$ iterations [31], $V_i^{\max}$ and $V_i^{\min}$ converge to the coalition maximum voltage $V_a^{\max}$ and minimum voltage $V_a^{\min}$.

2.3.2 Coalition Updating

Having gathered these data, each PV inverter follows the decision logic of Fig. 2.2 to determine if the coalition it currently belongs to needs to be divided, refined or left intact. Fig. 2.3 shows the transformation of the coalition under different updating actions.

Algorithm 1 Algorithm for assessing coalition voltage status

Initialization: $V_i^{\max}(0) = V_i$ and $V_i^{\min}(0) = V_i$

Iteration: At the kth iteration:

Step 1: Sends $V_i^{\max}(k)$ and $V_i^{\min}(k)$ to neighbors $j \in \mathcal{N}_i^a$

Step 2: Receives $V_j^{\max}(k)$ and $V_j^{\min}(k)$ from neighbors $j \in \mathcal{N}_i^a$

Step 3: Updates these two variables as follows:

$$\begin{cases} V_i^{\max}(k+1) = \max(V_i^{\max}(k), V_{j\in\mathcal{N}_i^a}^{\max}(k)) \\ V_i^{\min}(k+1) = \min(V_i^{\min}(k), V_{j\in\mathcal{N}_i^a}^{\min}(k)) \end{cases} \tag{2.3}$$

where $\mathcal{N}_i^a = \{j \in \mathcal{V}_a : (i,j) \in \mathcal{E}_a\}$ is the set of inverter i's neighbors within the same coalition as i.

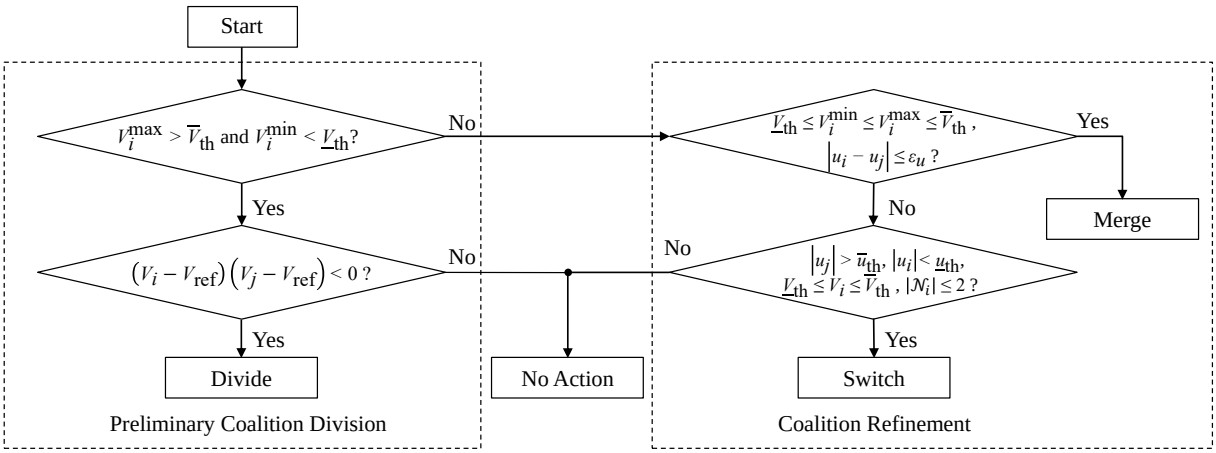

Figure 2.2: Decision logic for updating the coalitions.

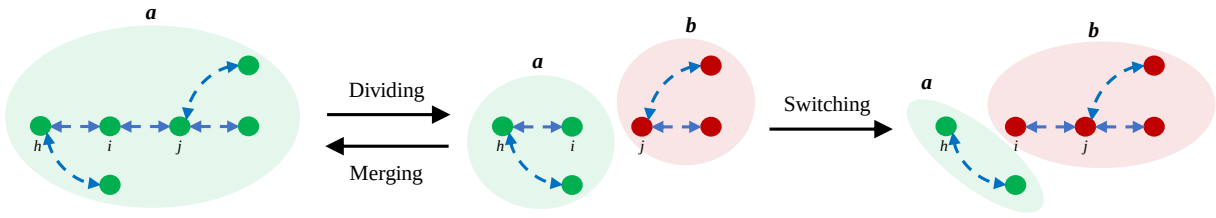

Figure 2.3: Coalition transformation under different updating actions.

a) Dividing: PV inverter i, $i \in \mathcal{G}_a$ first compares the coalition maximum voltage $V_i^{\max}$ and minimum voltage $V_i^{\min}$ with the upper and lower voltage thresholds, $\bar{V}_{\text{th}}$ and $\underline{V}_{\text{th}}$, to determine whether over and under-voltage problems coexist in the coalition. If this is the case, inverter i will decide to separate from its neighbor j, $j \in \mathcal{G}_a$ if its local voltage magnitude V_i is lower than the voltage reference value V_{ref} while its neighbor j's is higher, or vice-versa. If inverter i decides to separate from j, j will draw the same conclusion. They will therefore ignore the information they receive from each other in the calculation of the utilization ratio. As they no longer cooperate, the coalition $\mathcal{G}_a$ is split. For the coalition communication network, this action is equivalent to the removal of the edge between nodes i and j. Since the communication network of a typical distribution network has a tree topology, the removal of edges decomposes the original communication network into disjoint sub-networks. Each of these smaller networks still forms a connected graph with tree topology and supports the interactions of PV inverters in the newly formed coalitions. This voltage-based coalition division rule ensures that the PV inverters experiencing an upper voltage limit violation can be separated from those experiencing a lower voltage limit violation. Moreover, the PV inverters whose voltage is closer to the upper voltage limit are generally grouped with the former, while the PV inverters whose voltage is closer to the lower voltage limit are grouped with the latter.

b) Merging: If no further division is needed for a coalition, the PV inverters execute the capacity-based coalition refinement rules to improve the distribution of voltage regulation capacity among coalitions. For example, when both the maximum and minimum voltages of a coalition $\mathcal{G}_a$ have returned to the threshold range $[\underline{V}_{\text{th}}, \bar{V}_{\text{th}}]$, PV inverter i, $i \in \mathcal{G}_a$ can reasonably assume the over/under-voltage problem that existed before has been solved and the coalition can merge with others to share their voltage regulation burden. Therefore, if an inverter had separated from a neighbor, it checks the utilization ratio u_j of that neighbor j, $j \in \mathcal{G}_b$. If the difference between u_j and its own utilization ratio u_i is smaller than a threshold ε_u, then inverter i determines that it is safe to merge $\mathcal{G}_a$ with $\mathcal{G}_b$. Since this merger does not cause a large change to the reactive power output of the PV inverters currently in $\mathcal{G}_a$,

this action would not create voltage problems for them. PV inverter i then reconnects with j, and thus $\mathcal{G}_a$ merges with $\mathcal{G}_b$. This action reconnects node i and j in the communication network, to form a larger connected network that supports the communications within the newly merged coalition.

c) Switching: A coalition $\mathcal{G}_a$ cannot merge as a whole with another coalition $\mathcal{G}_b$ if its voltage problems persist or the difference in their utilization ratio is too large. However, some inverters can switch from coalition $\mathcal{G}_a$ to $\mathcal{G}_b$ when $\mathcal{G}_b$ suffers from a lack of voltage regulation capacity. Assuming the utilization ratio of j, $j \in \mathcal{G}_b$ exceeds an upper threshold $\bar{u}_{\text{th}}$, that is, almost all the voltage regulation capacity has been used up in coalition $\mathcal{G}_b$. When j's neighbor i, $i \in \mathcal{G}_a$ detects this situation, it can switch to $\mathcal{G}_b$ and thus bring extra regulation capacity to $\mathcal{G}_b$ under two conditions: 1) The coalition $\mathcal{G}_a$ has extra capacity, i.e. $|u_i| < \underline{u}_{\text{th}}$. 2) This switch does not bring a new voltage problem to coalition $\mathcal{G}_b$, i.e. $\underline{V}_{\text{th}} \leq V_i \leq \bar{V}_{\text{th}}$. Moreover, to preserve the connectivity of a coalition's communication network, this switching action is limited to PV inverters with no more than two neighbors. For example, in Fig. 2.3, PV inverter i can switch to $\mathcal{G}_b$ when necessary, while j is not allowed to switch coalitions because this would split the communication network of $\mathcal{G}_b$. For the communication network, the impact of a switch is the same as removing the edge between node i and its neighbor $h \in \mathcal{G}_a$ while reconnecting node i with its other neighbor $j \in \mathcal{G}_b$. Neither action would impact the connectivity or the tree topology of the newly formed coalitions' communication networks.

If the above conditions are not satisfied, the PV inverter takes no action in this coalition formation time interval.

2.3.3 Discussion

The actions of individual PV inverters periodically update the coalitions to solve potential conflict between voltage regulation and reactive power sharing. Compared with other strategies, the main characteristics of this coalition formation scheme are as follows:

- This scheme provides a simple, clear and uniform decision logic to each PV inverter.

The execution of this logic immediately results in a unique set of coalitions. Other dynamic coalition formation schemes involve several rounds of negotiation between potential partners [32, 33], or require a coordinating agent to construct the coalition gradually by contacting every possible member sequentially [34].

- This scheme allows the inverters to flexibly organize themselves using dividing, merging and switching actions in response to real-time network operating condition. In contrast, centralized network decomposition-based strategies [35, 36] use the voltage sensitivity matrix to divide the network and the regulation resources. These approaches give inverters less flexibility to determine the scope of their cooperation.

2.4 Coordination within a Coalition

Once a coalition has been formed, the PV inverters within that coalition autonomously select one member as their leader. A feedback-based leader-follower consensus algorithm then coordinates the real-time control of the inverters. The leader adjusts its output to eliminate the voltage violation. The followers, i.e. the other inverters in the coalition, adjust their outputs correspondingly to share the regulation burden.

2.4.1 Role Identification

In existing leader-follower consensus control strategies, the system operator usually predetermines which inverter is most likely to experience the largest voltage deviation and selects it as the leader for the entire control process [23, 24, 25]. On the other hand, under our proposed control, the PV inverters first determine the largest voltage deviation within their coalition and then identify their roles accordingly. As in the coalition maximum voltage assessment process described in Algorithm 1, during a time window $[T,\, T + \Delta T]$ after the coalition formation, PV inverters exchange their local voltage deviations $\Delta V_i = |V_i - V_{\text{ref}}|$ with their neighbors and update their estimation of the coalition maximum voltage deviation $\Delta V_i^{\max}$. The PV inverter whose voltage deviation is the largest assumes the role of

leader, while the rest become followers.

2.4.2 Utilization Ratio Adjustment

a) Feedback Control: After role identification, the leader inverter of a coalition $\mathcal{G}_a$ takes its local voltage magnitude V_l as the feedback signal and adjusts its utilization ratio u_a at each iteration k as follows

$$u_a(k+1) = \underline{\lambda}(k) - \bar{\lambda}(k) \tag{2.4}$$

$$\bar{\lambda}(k+1) = [\bar{\lambda}(k) + \alpha(V_l(k) - \bar{V})]^+ \tag{2.5}$$

$$\underline{\lambda}(k+1) = [\underline{\lambda}(k) + \alpha(\underline{V} - V_l(k))]^+ \tag{2.6}$$

where $\bar{\lambda}$ and $\underline{\lambda}$ are control states. α is the step-size parameter. $[*]^+$ denotes the projection operator onto $[0, +\infty)$. This calculation is similar to an integral controller with a dead-band. When the local voltage magnitude exceeds the upper voltage limit, the leader inverter reduces its utilization ratio u_a and hence its reactive power output. On the other hand, if the local voltage magnitude is too low, it increases its utilization ratio to support the voltage.

b) Leader-follower Consensus Algorithm: The utilization ratio determined by the leader inverter is then communicated within coalition $\mathcal{G}_a$ according to the logic shown in Algorithm 2. At each iteration, inverter i sends its utilization ratio to its neighbors in the same coalition and receives their utilization ratios. It then updates its utilization ratio to be the average of its own and its neighbors' utilization ratio. Since the communication network for the coalition is connected, a consensus on the utilization ratio u_a will be reached globally and exponentially [37].

c) Reactive Power Output: The maximum available reactive power capacity of PV inverter i is constrained by its rated capacity S_i^r and real-time active power output P_i:

$$Q_i^{\max} = \sqrt{S_i^{r2} - P_i^2}. \tag{2.8}$$

Since PV inverters are typically oversized, they can provide reactive power compensation

Algorithm 2 Algorithm for adjusting the utilization ratio

Iteration: At the kth iteration:

Step 1: Sends $u_i(k)$ to neighbors $j \in \mathcal{N}_i^a$

Step 2: Receives $u_j(k)$ from neighbors $j \in \mathcal{N}_i^a$

Step 3: Updates the utilization ratio:

$$u_i(k+1) = \frac{1}{1+|\mathcal{N}_i^a|}\left[u_i(k) + \sum_{j\in\mathcal{N}_i^a} u_j(k)\right]. \tag{2.7}$$

even when they generate their rated active power output P_i^r,

$$S_i^r = (1+\beta)P_i^r \tag{2.9}$$

where β is the over-sizing percentage. Based on the utilization ratio, the reactive power contribution from PV inverter i for voltage regulation is

$$Q_i(k) = [u_i(k)]_{-1}^{1} Q_i^{\max} \tag{2.10}$$

where $[*]_{-1}^{1}$ denotes the projection operator onto the utilization ratio limit set $[-1, 1]$.

2.4.3 Algorithm Analysis

In this subsection, we demonstrate the analytical connections between the feedback-based leader-follower consensus algorithm and distributed optimization algorithms.

Within a coalition, the voltage regulation can be formulated as the following optimization problem:

$$\begin{aligned} \min \quad & \sum_{i\in\mathcal{G}_a} \frac{1}{2}\gamma_i Q_i^2 \\ \text{s.t.} \quad & \underline{V} \le V_l \le \bar{V} \\ & Q_i \in \mathcal{Q}_i,\ \forall i \in \mathcal{G}_a \end{aligned} \tag{2.11}$$

where $\gamma_i > 0$ is a penalty parameter associated with the reactive power output of inverter i and $\mathcal{Q}_i = [-Q_i^{\max}, Q_i^{\max}]$. The local voltage magnitude of the leader inverter can be approximated by linearizing the power-flow equation as:

$$V_l \approx \sum_{i \in \mathcal{G}_a} \frac{\partial V_l}{\partial Q_i} Q_i + V_{\text{uncon}} \tag{2.12}$$

where $\frac{\partial V_l}{\partial Q_i} > 0$ is the sensitivity of the local voltage at the leader inverter to the reactive power output of inverter i. V_{uncon} is the uncontrollable part of the voltage magnitude, which depends on the load and active PV generation.

Assuming problem (2.11) is feasible and the Slater condition is satisfied, i.e. there exist Q_i, $\forall i \in \mathcal{G}_a$ such that $Q_i \in \mathcal{Q}_i$ and $\underline{V} < V_l < \bar{V}$. Given the strong convexity of the cost function, this problem has a unique optimal solution which can be obtained using a projected primal-dual dynamics feedback optimization algorithm [38]:

$$\dot{Q}_i = \Pi_{\mathcal{T}_{\mathcal{Q}_i}^{Q_i}} \left[-\gamma_i Q_i + \frac{\partial V_l}{\partial Q_i} (\underline{\lambda} - \bar{\lambda}) \right], \ \forall i \in \mathcal{G}_a \tag{2.13}$$

$$\dot{\bar{\lambda}} = \Pi_{\mathcal{T}_{\mathbb{R}_+}^{\bar{\lambda}}} (V_l - \bar{V}) \tag{2.14}$$

$$\dot{\underline{\lambda}} = \Pi_{\mathcal{T}_{\mathbb{R}_+}^{\underline{\lambda}}} (\underline{V} - V_l) \tag{2.15}$$

where $\bar{\lambda}$, $\underline{\lambda} \in \mathbb{R}_+$ are the dual variables for the upper and lower voltage limit constraints in problem (2.11). Due to the special structure of the objective function in problem (2.11), as proved in [21], (2.13) can be simplified as

$$Q_i = \left[\gamma_i^{-1} \frac{\partial V_l}{\partial Q_i} (\underline{\lambda} - \bar{\lambda}) \right]_{-Q_i^{\max}}^{Q_i^{\max}}, \ \forall i \in \mathcal{G}_a. \tag{2.16}$$

Assuming in problem (2.11), $\gamma_i = (Q_i^{\max})^{-1} \frac{\partial V_l}{\partial Q_i}$. (2.16) becomes

$$u_i = \frac{Q_i}{Q_i^{\max}} = \left[(\underline{\lambda} - \bar{\lambda}) \right]_{-1}^{1}, \ \forall i \in \mathcal{G}_a. \tag{2.17}$$

To execute this "gather and broadcast" algorithm under the neighboring communication constraint, different distributed algorithms have been proposed [21, 38]. The algorithm we implement is similar to the method in [38]. The leader inverter (i.e., actuators who access

sensor data in [38]) measures its local voltage and updates the dual variables $\bar{\lambda}$, $\underline{\lambda}$ according to (2.14) and (2.15). The discrete-time version of this process is (2.5) and (2.6). For the update of the utilization ratio, the leader inverter has direct access to $(\underline{\lambda} - \bar{\lambda})$ and is thus able to adjust its utilization ratio according to (2.17), i.e., (2.4) in discrete-time. However, the followers (i.e., actuators who do not access sensor data in [38]) rely on the peer-to-peer communication to pass the dual variables $(\underline{\lambda} - \bar{\lambda})$ from the leader. Therefore, they keep a local copy $(\underline{\lambda} - \bar{\lambda})_i$ of $(\underline{\lambda} - \bar{\lambda})$ and update this local copy when information arrives from their neighbors. That is, the follower inverters preserve their own utilization ratio u_i and update this value iteratively as described in Algorithm 2. It is proved in [38] that this modified algorithm is guaranteed to converge to the optimal solution when the coupling in the communication graph is sufficiently strong. The feedback-based leader-follower consensus algorithm is thus able to eliminate upper or lower voltage limit violations within the coalition effectively and the utilization ratio converges to the optimal solution of problem (2.11). The detailed convergence proof can be found in [38].

2.5 Implementation

With their increased deployment, distributed energy resources (DERs) play a more active role in system operation. Various stakeholders have been developing standards to specify DER interconnection criteria and requirements (e.g., IEEE 1547-2018), as well as to guide DER interoperability and communication (e.g., IEEE 1815, IEEE 2030.5, IEC 61850). Accordingly, inverters are evolving towards more advanced, standardized and autonomous functionalities, which makes their cooperative control actions possible [12]. For example, a project by the Toronto and Region Conservation Authority (TRCA) demonstrated the practicality of organizing the smart inverters under a multi-agent peer-to-peer communication framework for distribution network voltage regulation [39]. Our proposed voltage regulation strategy coordinates the smart PV inverters located on the low-voltage network under a similar framework. For large-scale deployment, considering there are abundant utility-owned voltage regulation devices on the primary side and the cost for communication, it is recom-

mended to divide the distribution network and implement the strategy on each low-voltage network independently. An important obstacle is that these inverters are usually owned by utility customers. The utility would therefore not be able to coordinate their actions directly. To address this issue and encourage the participation of smart inverters in voltage regulation, incentive schemes [40] and alternative forms of inverter ownership [41] are being considered. Since the proposed strategy supports flexible plug-and-play operation, it can accommodate a variable number of inverters.

2.6 Case Study

2.6.1 Test System

Fig. 2.4 shows the single-line diagram of the balanced 230/400V 103-node radial distribution network used to demonstrate the performance of the proposed control strategy. The squares, circles and dashed lines represent the load nodes, PV nodes and the communication links, respectively. This network was extended based on the topology of a real semi-urban feeder in Flanders, Belgium. Its detailed network parameters can be found in [42]. To assess the effectiveness of the proposed strategy in a network where the load and PV generation are very unevenly distributed, we connected four heavy loads (a school, a bank, a grocery store and an office) at nodes 38, 56, 58, 96. Two small PV farms are located at nodes 69 and 76. Sixty houses are connected to the network, 30 of which are equipped with PV inverters. The 1-minute-resolution daily profiles for the PV generation and residential consumption were constructed based on the Pecan Street data set of June 16, 2014 [43]. The commercial load profiles are from [44]. Fig. 2.5 shows the normalized load and PV generation profiles. Table 2.1 gives the capacity of these loads and DERs. According to the European Standard EN50160, the maximum allowable voltage deviation for this network is $\pm 10\%$. Fig. 2.6 shows the voltage profiles of the distribution network when the only regulation device is the distribution transformer. This transformer raises the system voltage during periods of heavy load and lowers the system voltage when the PV generation creates a high reverse power

flow, i.e., from 10:00 to 16:30. However, during this period, even when the voltage at the end of laterals 1 and 4 hovers around the lower voltage limit, the voltage at the end of lateral 3 exceeds the upper voltage limit.

Although the analysis of the leader-follower consensus algorithm is built on a linearized power flow model, the power system is simulated using a full nonlinear AC power flow model based on MATPOWER [45]. The voltage regulation coalitions are reformed every 5 minutes and the sampling period of the local controllers is 200 milliseconds. To mitigate the impact of the volatility in PV generation, the voltage information gathered for coalition formation is its moving average value over a 15-minute rolling window. The control strategy regulation range $[\bar{V}, \underline{V}]$ also reserves a small buffer. Moreover, as the coalition formation is taken as a preventive action, the threshold range $[\bar{V}_{\text{th}}, \underline{V}_{\text{th}}]$ is set to be more conservative than the regulation range. Table 2.2 gives the detailed parameters of the proposed control strategy. We demonstrate this strategy's effectiveness through a 24-hour simulation. It is then compared with a simple localized controller and a state-of-the-art centralized network decomposition-based actuator organization scheme. The robustness and the generalizability of the proposed strategy are also assessed.

Table 2.1: Capacity of the Load and DERs

Type	Houses	School	Bank	Grocery
Size (kW)	2.2–14.5	68.4	31.4	45.1
Type	Office	Residential PV	PV Farm 69	PV Farm 76
Size (kW)	62.3	2.5–7.5	45.5	140.0

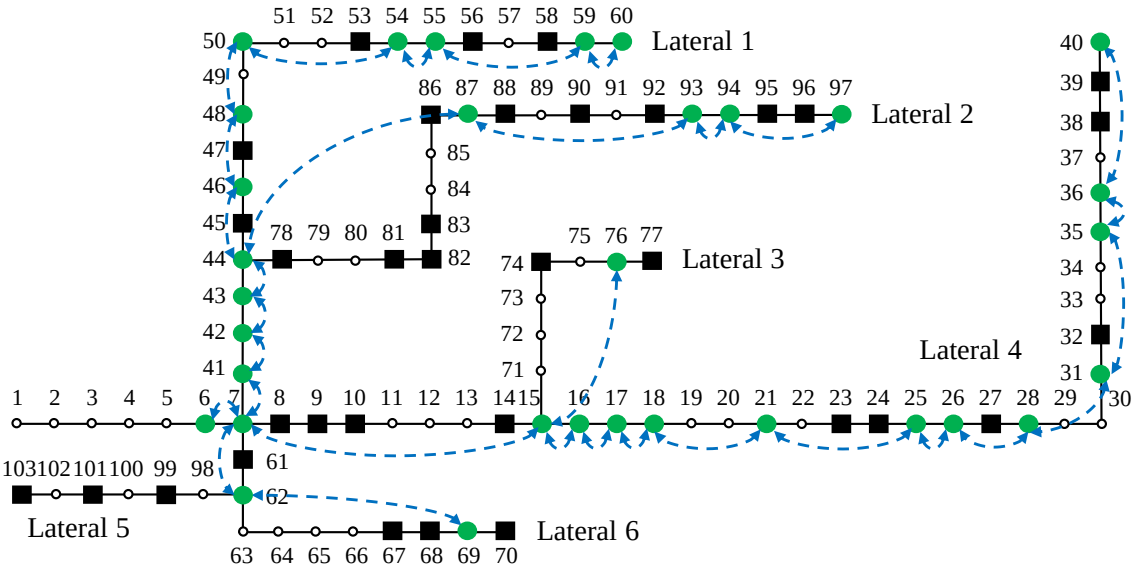

Figure 2.4: Single-line diagram of the test system.

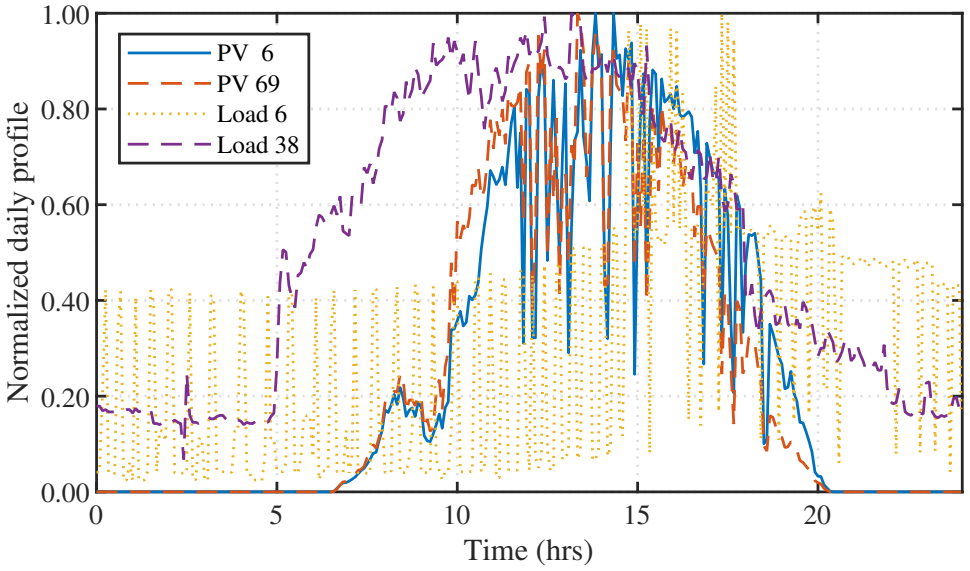

Figure 2.5: Normalized daily profiles of the PV located on node 6, 69 and the load located on node 6, 38.

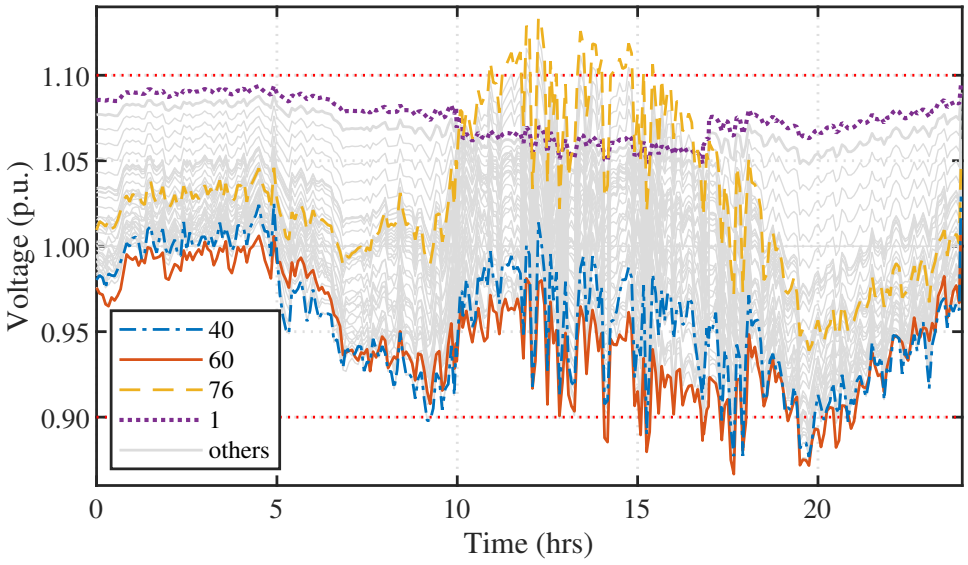

Figure 2.6: Voltage profiles of the network without PV reactive power compensation over a 24-hour period.

Table 2.2: Parameters of the Control Strategy

$\bar{V}_{\text{th}}$	$\underline{V}_{\text{th}}$	$\bar{V}$	$\underline{V}$	V_{ref}
1.05 p.u.	0.95 p.u.	1.09 p.u.	0.91 p.u.	1.00 p.u.
ε_u	$\bar{u}_{\text{th}}$	$\underline{u}_{\text{th}}$	α	β
0.02	0.90	0.70	20	0.10

2.6.2 Performance Analysis

a) Convergence and Accuracy: Fig. 2.7 shows the iteration process of the PV inverters assuming that the load and PV generation remain static at the values they have at 9:07. At this time, all the PV inverters belong to the same coalition and they work together in about 100 iterations, i.e. 20 seconds, to bring the voltage at node 40 back up to the prescribed

lower voltage limit of 0.91 p.u. Meanwhile, the utilization ratio of each inverter gradually converges to the value determined by the leader inverter. The red dashed lines show the optimal solution of problem (2.11) where the voltage sensitivity value is calculated based on the Jacobian matrix, and the power flow equation constraints are modeled with the AC power flow model under Second-Order Cone Programming (SOCP) relaxation [46]. The leader-follower consensus algorithm drives the system to the optimal solution of problem (2.11), which confirms the analytical connection discussed in Section 2.4.

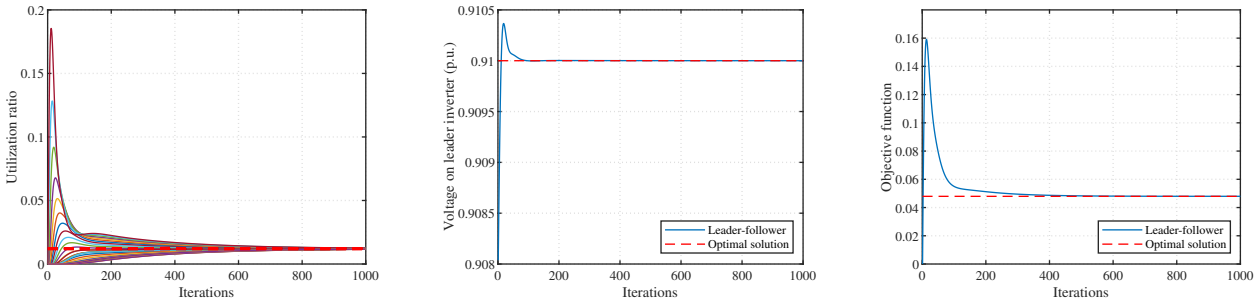

(a) (b) (c)

Figure 2.7: Iteration process of the feedback-based leader-follower consensus algorithm. (a) Utilization ratios of each inverter, (b) Voltage magnitude at the leader inverter, (c) Objective function of problem (2.11)

.

b) Control over a 24-hour period: Fig. 2.8 illustrates the voltage regulation achieved by the proposed control strategy over the course of a day and demonstrates how the PV inverters are able to form into coalitions autonomously and solve the voltage violation problems cooperatively. Fig. 2.9 shows the coalitions that were formed at 15:15. Coalition 1 consists mainly of PV inverters on laterals 1 and 2, coalition 2 covers the inverters located on laterals 3, 6 and the first half of lateral 4. Inverters on the second half of lateral 4 form coalition 3. These coalitions evolve based on real-time voltage measurements. For example, coalition 3 reunites with coalition 2 to help solve its over-voltage problem at noon. However, this only

happens when the voltages within coalition 3 are inside a safe range. Otherwise, coalition 3 separates from coalition 2 to prevent suffering from a lower voltage limit violation. In addition, coalitions can also be refined by the switching action of individual inverters. For instance, inverter 41 switches from coalition 2 to coalition 1 at 15:15 when coalition 1 lacks sufficient regulation capacity. Most of the time, coalitions 1, 2, 3 are led by inverters 60, 76, and 40, respectively.

2.6.3 Comparison with Other Approaches

a) Local Control: When all the communication links are removed, the proposed strategy reduces to a simple local controller, the same as the one proposed in [47]. In this case, each coalition contains a single inverter, which measures its local voltage and adjusts its reactive power output based on (2.4)-(2.6). Fig. 2.10 shows that this local control strategy is able to improve the voltage profile. However, lower voltage limit violations persist, mainly caused by the saturation of the PV inverters reactive power capacity. For example, during the time interval 15:13–15:19, only PV inverters 55, 59, 60 detect an under-voltage problem on lateral 1 and produce reactive power to solve it. However, due to their limited capacity and while their utilization ratios rise to the upper limit of 1.0, (i.e. they produce maximum reactive power), this voltage violation problem persists. To solve this problem, the active power generation from these PV inverters might need to be curtailed, which would lead to an economic loss for their owners. This problem does not occur with the proposed control strategy because coalition 1 in Fig. 2.9 involves more PV inverters that can help deal with these low voltages. Moreover, throughout the entire control process, only the PV inverters installed at the end of laterals actively participate in voltage regulation. Frequent actions and large reactive power output can affect the lifetime of these inverters [48]. In contrast, the reactive power capacity of the rest of PV inverters is barely used.

b) Centralized Organization Scheme: In the centralized actuator organization scheme proposed in [35], a central agent derives the sensitivity matrix A from the Jacobian matrix

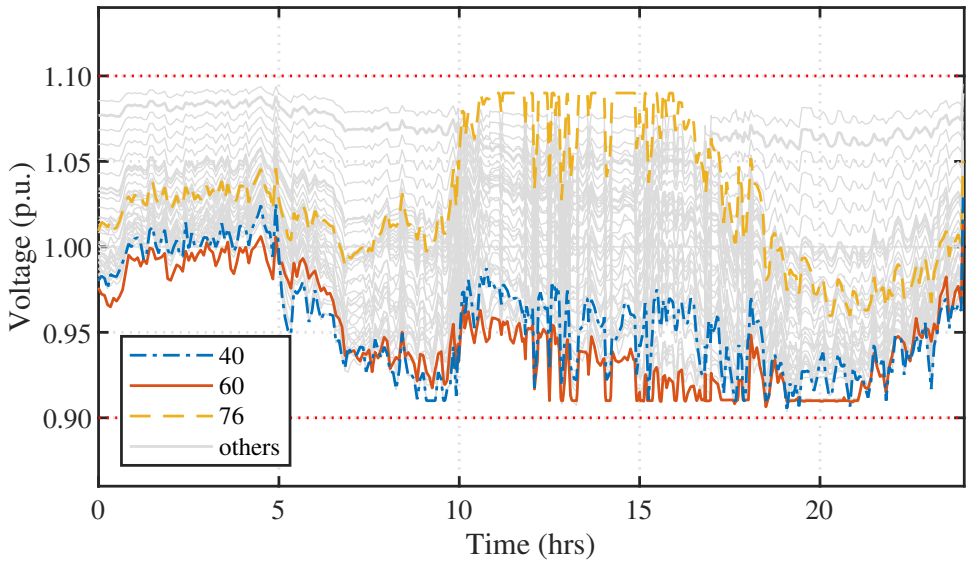

(a)

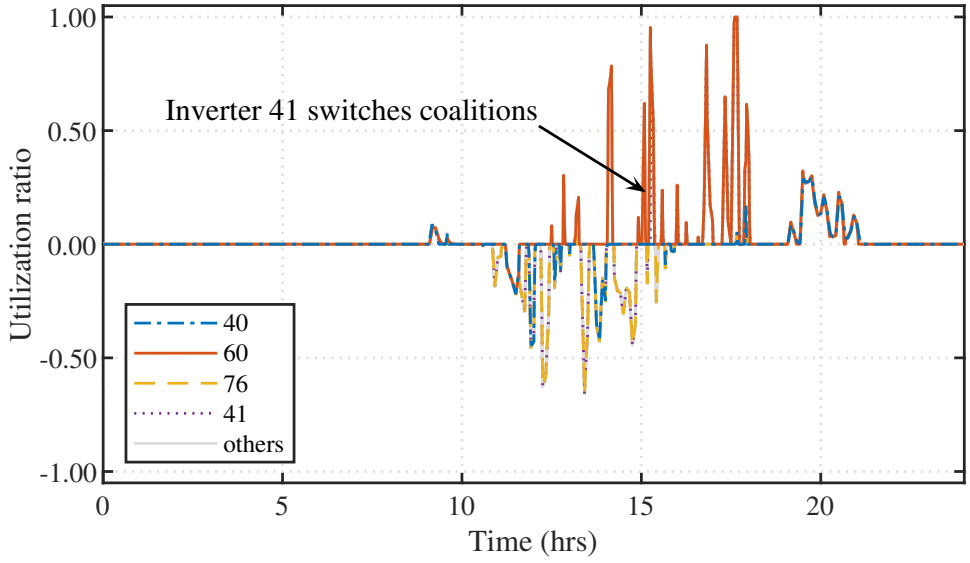

(b)

Figure 2.8: Voltage regulation results of the proposed control strategy. (a) 24-hour voltage profiles; (b) Utilization ratios.

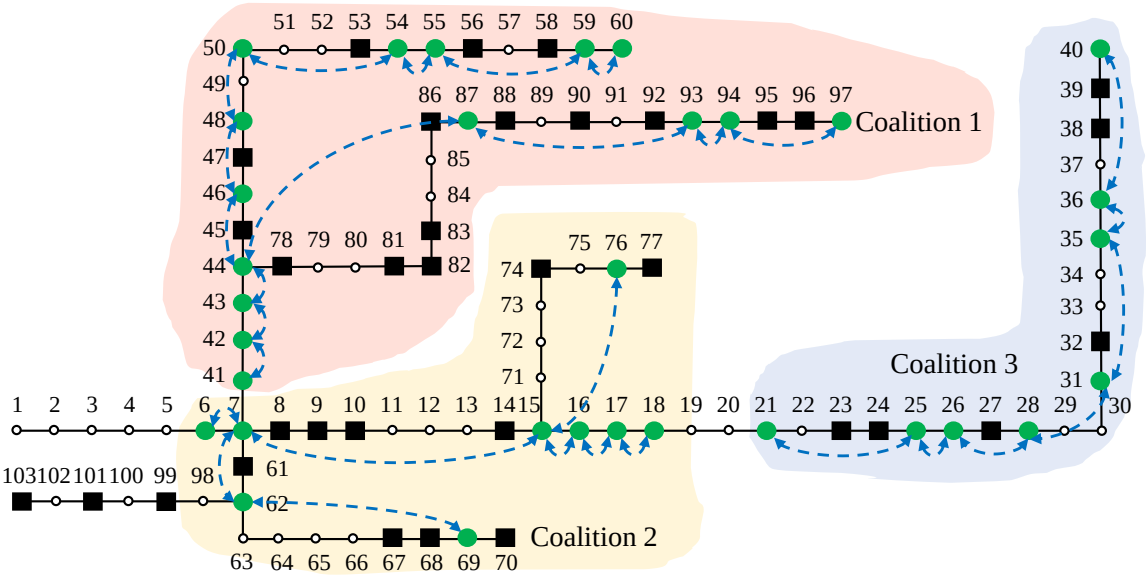

Figure 2.9: Voltage regulation coalitions under the proposed strategy at 15:15.

of the Newton-Raphson power flow solution:

$$\begin{pmatrix} \Delta\theta \\ \Delta V \end{pmatrix} = \begin{pmatrix} A_{\theta P} & A_{\theta Q} \\ A_{VP} & A_{VQ} \end{pmatrix} \begin{pmatrix} \Delta P \\ \Delta Q \end{pmatrix} = A \begin{pmatrix} \Delta P \\ \Delta Q \end{pmatrix}. \tag{2.18}$$

This agent then applies epsilon decomposition to A_{VQ}:

$$A_{VQ} = A'_{VQ} + \varepsilon B \tag{2.19}$$

which decomposes the original voltage magnitude-reactive power sensitivity matrix A_{VQ} into strong couplings A'_{VQ} and weak couplings B. The weak couplings, i.e. any element less than ε, in A_{VQ} are then set to 0. Correspondingly, the weakly coupled nodes in the network, and the inverters on these nodes, are partitioned into different voltage regulation zones. The central agent controls the partition result by updating the magnitude of ε between 0 and 1. If $\varepsilon = 0$, all nodes are considered as strongly coupled and there is no partition, while if $\varepsilon = 1$, there is no cooperation. For comparison, we replace our coalition formation with this scheme. The central agent checks the network voltage magnitudes every 5 minutes. If

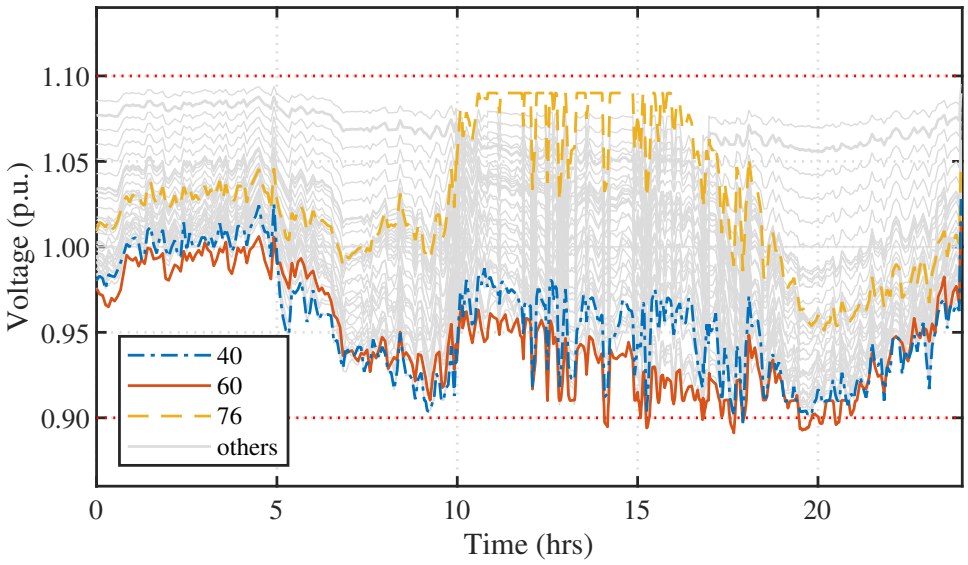

(a)

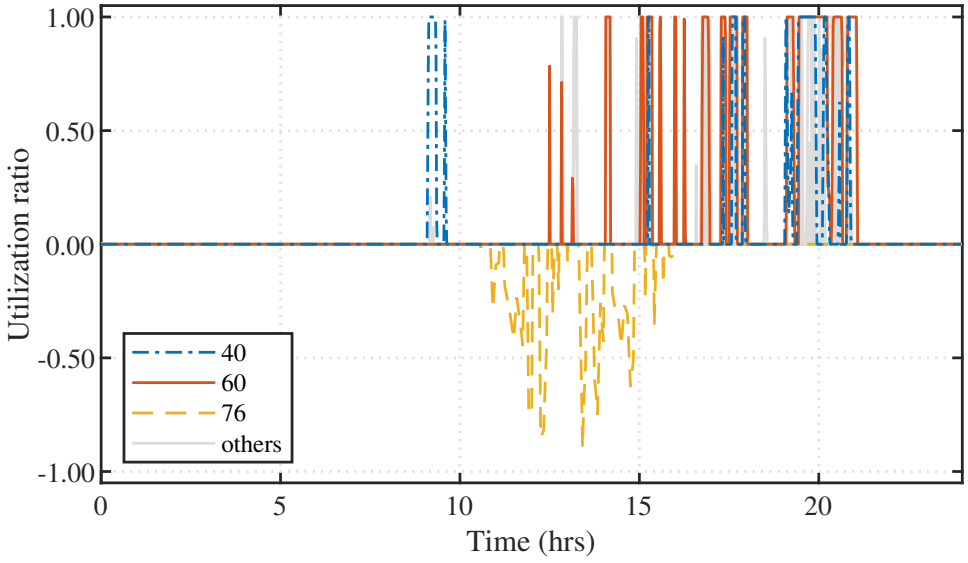

(b)

Figure 2.10: Voltage regulation results of the local control strategy. (a) 24-hour voltage profiles; (b) Utilization ratios.

a voltage threshold is violated, it initiates the partition and selects the smallest ε to ensure that the inverters whose local voltage is higher than $\bar{V}_{\text{th}}$ can be separated from those inverters whose local voltage is lower than $\underline{V}_{\text{th}}$. The leader-follower consensus algorithm still guides the within-coalition coordination. Fig. 2.11 shows the corresponding voltage regulation results. Similar to our proposed scheme, this scheme is able to organize the inverters in different groups to solve the voltage violation problems. However, this coupling strength-based scheme is essentially different from our real-time voltage/capacity-based coalition formation scheme. Fig. 2.12 illustrates this difference. At 15:15, inverter 40 needs to be separated from inverter 76. Under our scheme, this separation is completed as inverter 18 separates from inverter 21 based on their voltage magnitudes. However, under the coupling strength-based scheme, the central agent finds the weakest coupling is between nodes 15 and 16 and sets the ε value correspondingly to remove this coupling. However, couplings weaker than this ε, e.g. the coupling between 46 and 48, are also removed, which results in a smaller coalition 1 than ours. In general, with this network decomposition-based actuator organization scheme, inverters that are closer to the substation, and thus have a weaker coupling with their neighbors, are prone to be excluded from any cooperation.

2.6.4 Robustness

a) Communication Latency: Communication latency is inevitable in real-world implementations. One way to handle the latency is to allocate a longer time for each iteration. To analyze the robustness of the proposed approach in handling latency, we increased the sampling period to 10 times its original value, i.e. 2000 milliseconds. Fig. 2.13 shows the voltage regulation results. In this case, the coalition formation is barely impacted. This is because the coalitions are updated every 5 minutes, which allows the inverters sufficient time to assess the coalition voltage status and make decisions. On the other hand, it becomes more difficult for the inverters within the same coalition to fully communicate and reach consensus on their utilization ratios, particularly when the size of the coalition is large. For example, when all the inverters return to the same coalition after 20:00, discrepancies in the utilization

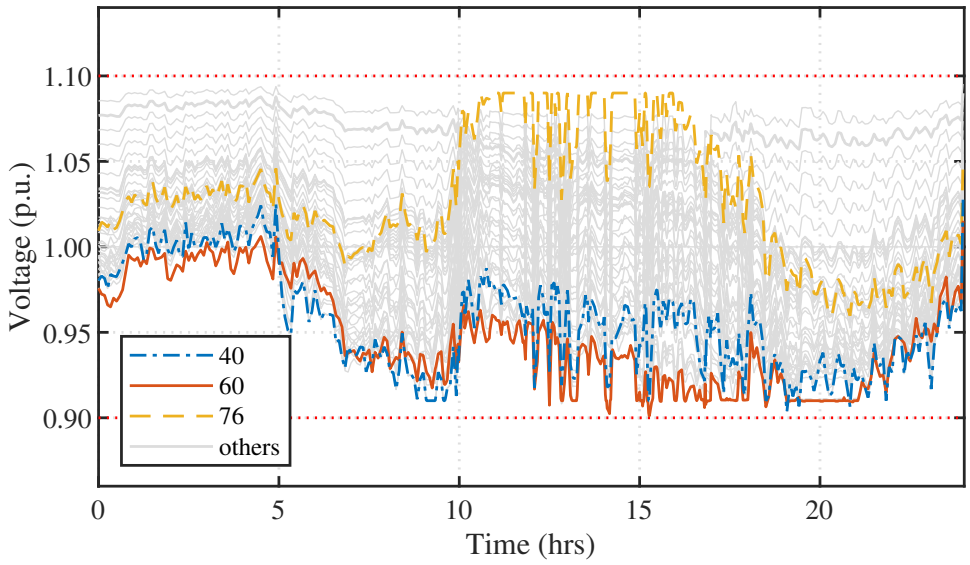

(a)

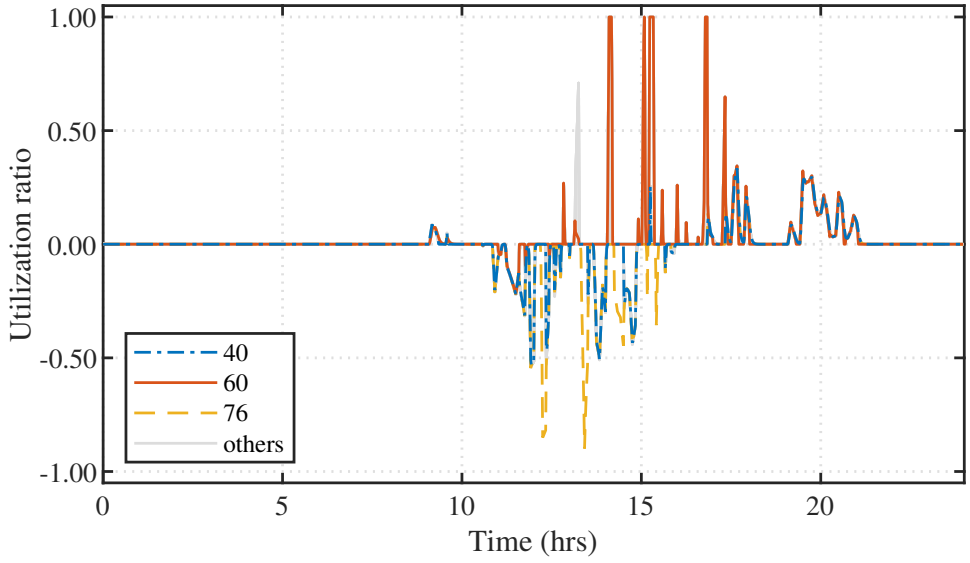

(b)

Figure 2.11: Voltage regulation results with the centralized organization scheme. (a) 24-hour voltage profiles; (b) Utilization ratios.

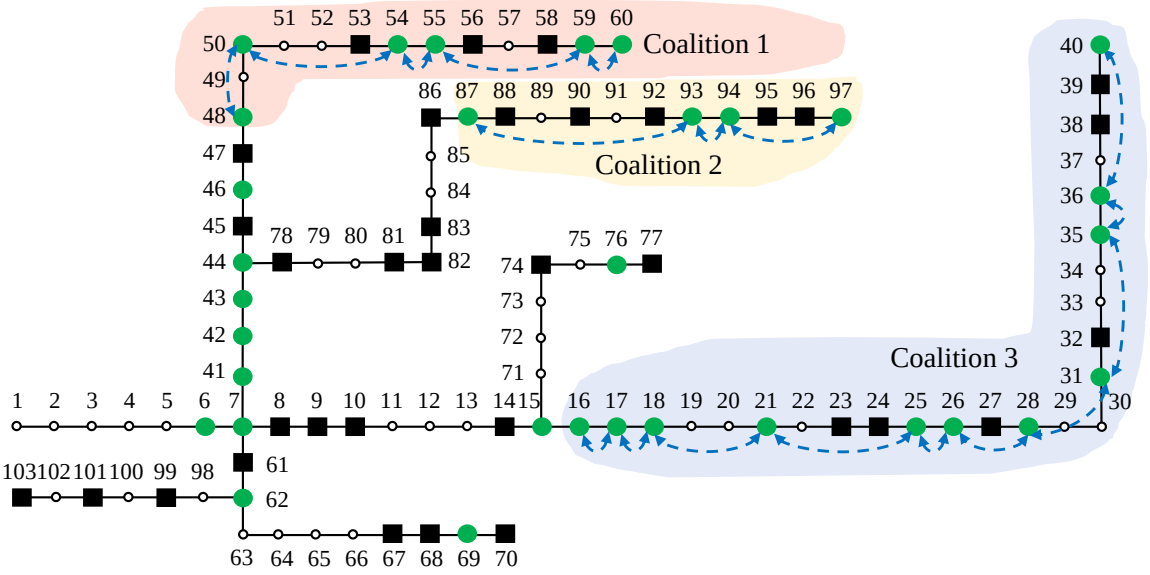

Figure 2.12: Voltage regulation coalitions under centralized organization scheme at 15:15.

ratio become obvious. However, the trends in these utilization ratios remain similar and the voltage regulation results are almost the same as in the normal case.

b) Communication Failure: Communication failure is another problem that can deteriorate the effectiveness of the proposed strategy. For the robustness test, we assume that 10% of the communication links fail at random every hour and these failure last for 15 minutes. For the inverters, a communication link failure is similar to a coalition division, as two neighboring inverters no longer cooperate. The difference is that the separated inverters are no longer able to merge or switch to each other's coalition since no information can be transmitted between them. Once the communication resumes, these actions are possible again. Fig. 2.14 shows the voltage regulation results. In this case, as the unnecessary "coalition division" happens frequently, the scopes of cooperation are intermittently constrained. Therefore, the utilization ratios are quite different from the normal case and the coalition regulation capacity insufficiency problem can occur. However, as an adaptive coalition formation scheme, the proposed strategy is able to handle those undesirable separations when

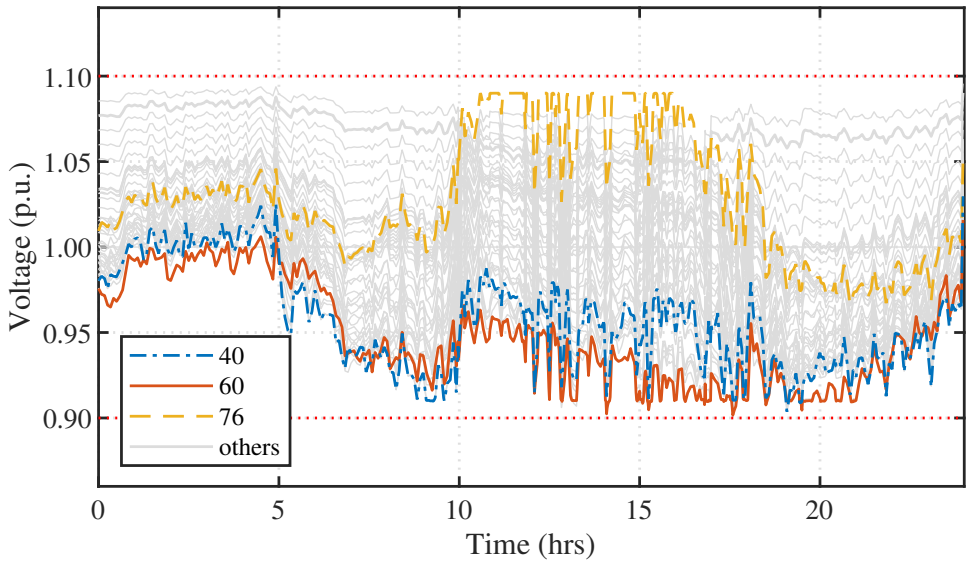

(a)

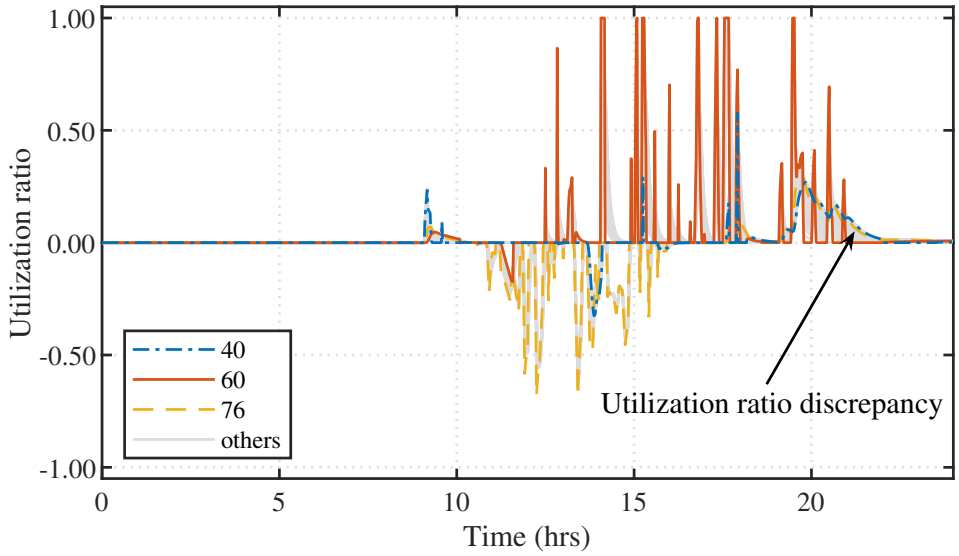

(b)

Figure 2.13: Voltage regulation results under communication latency. (a) 24-hour voltage profiles; (b) Utilization ratios.

the communication recovers. The voltage magnitude can still be effectively constrained.

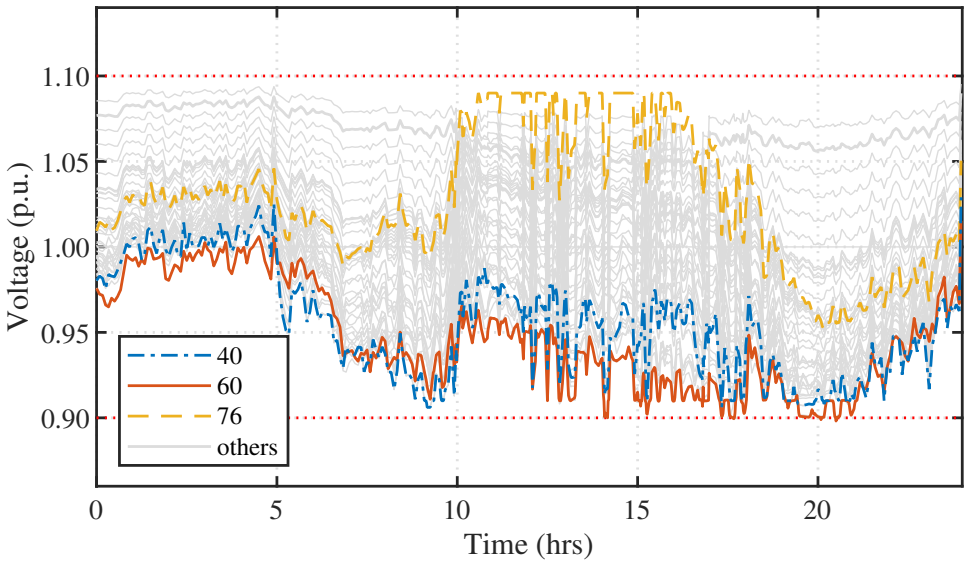

(a)

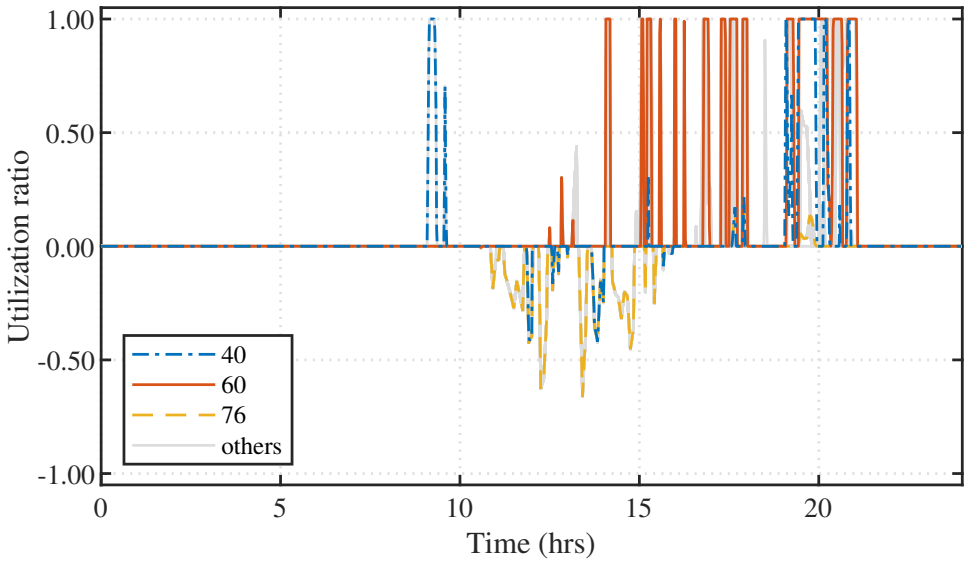

(b)

Figure 2.14: Voltage regulation results under communication failure. (a) 24-hour voltage profiles; (b) Utilization ratios.

2.6.5 Generalizability

To test the extent to which the proposed approach can be generalized, we created 50 different network scenarios with varying inverter locations, quantities and capacities. In the construction of each case, 60 houses, 20–40 of which are equipped with smart PV inverter, are randomly sampled out of 167 candidate profiles from the Pecan Street data set. These houses are then randomly allocated to the 103-node network. For comparison, the local control strategy and the centralized organization scheme are also tested. In the simulations, as the over-voltage problem always occurs on lateral 3 and the abundant inverter reactive power resources of the small farm located at node 76 can effectively solve this problem, the over-voltage limit violation comparison results are not presented here. Fig. 2.15 shows the average daily lower voltage limit violations. All three control strategies are able to improve the voltage profiles. However, as the local control suffers from inverter saturation problems, the average daily lower voltage limit violation time under this control is as high as 27.5 minutes. On the other hand, this value reduces to 4.6 minutes and 3.6 minutes when the centralized organization scheme or the proposed strategy is implemented. This is because these two strategies are able to coordinate the inverters for voltage regulation, and mitigate the insufficiency in local control resources. Furthermore, the proposed strategy achieves slightly better performance than the centralized organization scheme as it is able to organize the inverters in a more flexible way.

2.7 Implementation in Unbalanced Networks

To assess the effectiveness of the proposed strategy in unbalanced networks, we modeled the IEEE European LV test feeder in OpenDSS [49]. The detailed network parameters and customer loading profiles can be found in [50]. We extended this network by connecting the bank and the office load described in Section 2.6 at nodes 819 and 881. A small PV farm with a capacity of 28 kW at each phase is connected at node 617. The smart PV inverters are allocated to 10, 7 and 9 randomly selected houses on phases a, b and c, respectively.

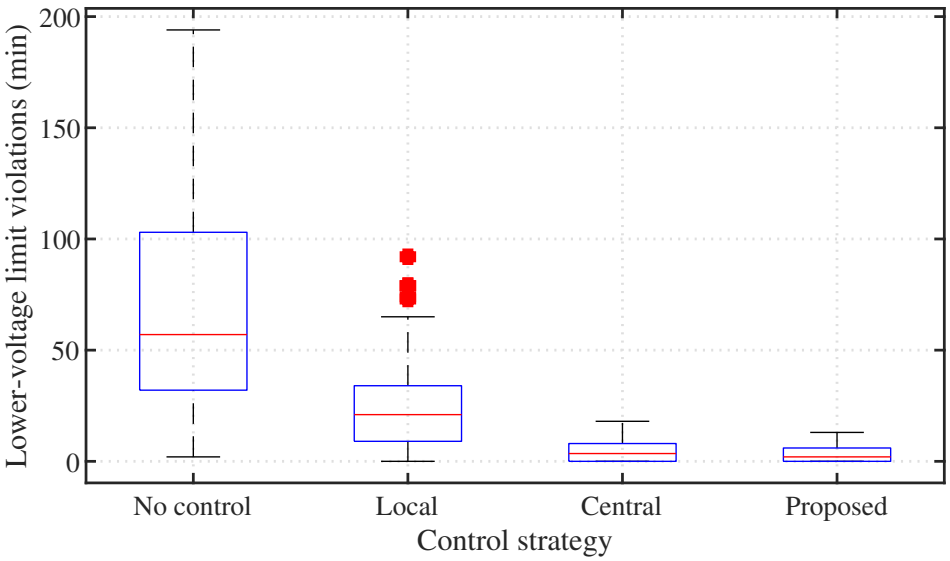

Figure 2.15: Average daily lower-voltage limit violations under varying network settings with different control strategies.

The daily PV generation profiles are the same as described in Section 2.6. Fig. 2.16 shows the modified test feeder. To maintain the voltage deviation within $\pm 5\%$ [25, 26], we set the regulation range $[\bar{V}, \underline{V}]$ as $[1.049, 0.951]$, the threshold range $[\bar{V}_{\text{th}}, \underline{V}_{\text{th}}]$ as $[1.025, 0.975]$. The other parameters are as in Table 2.2. We implemented the proposed control strategy in each phase separately.

Fig. 2.17 demonstrates that the proposed strategy effectively improves the voltage profiles. Fig. 2.18 shows the coordinated actions of the smart PV inverters over the day. During the control process, the PV inverters at phase a mainly form two coalitions since inverter 349 separate from inverter 629 at 10:45. These two coalitions are led by inverters 617 and 898 to solve their over-voltage and under-voltage problems. On the other hand, the PV inverters in phase b remain in the same coalition the whole day while the coalition leader changes. For example, inverter 899 leads the coalition to eliminate the lower voltage limit violations from 9:25 to 10:25, while inverter 617 takes the leader position in the middle of the day to solve the over-voltage problems. The PV inverters on phase c belong to the same coalition

for most of the time. However, inverter 539 separates from inverter 342 at 13:45 and thus inverter 539, 778, 701 and 780 stop absorbing reactive power until 14:00. This happens as the voltage of these inverters are relatively low during this period.

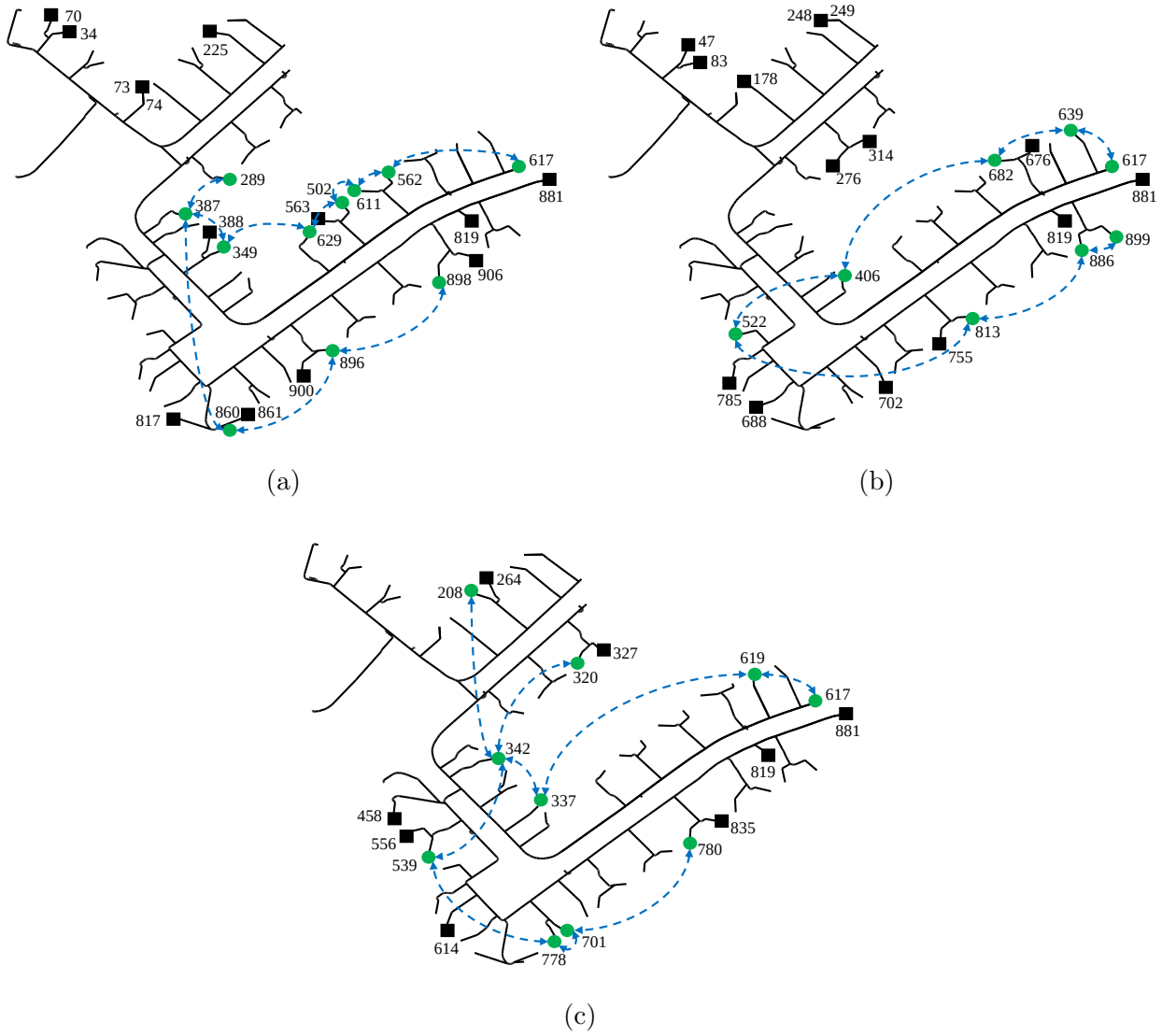

Figure 2.16: Diagrams of the unbalanced test feeder. (a) Phase a, (b) Phase b, (c) Phase c

.

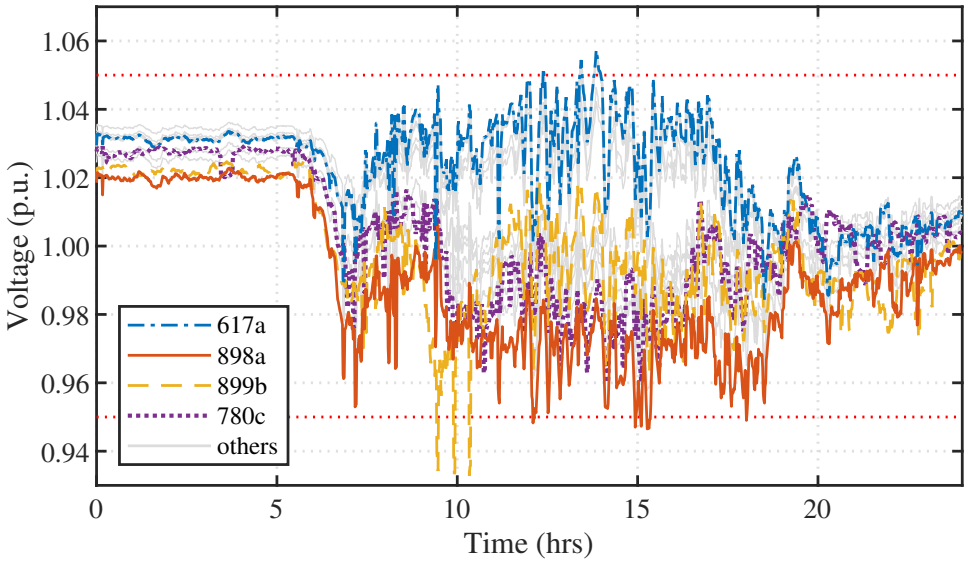

(a)

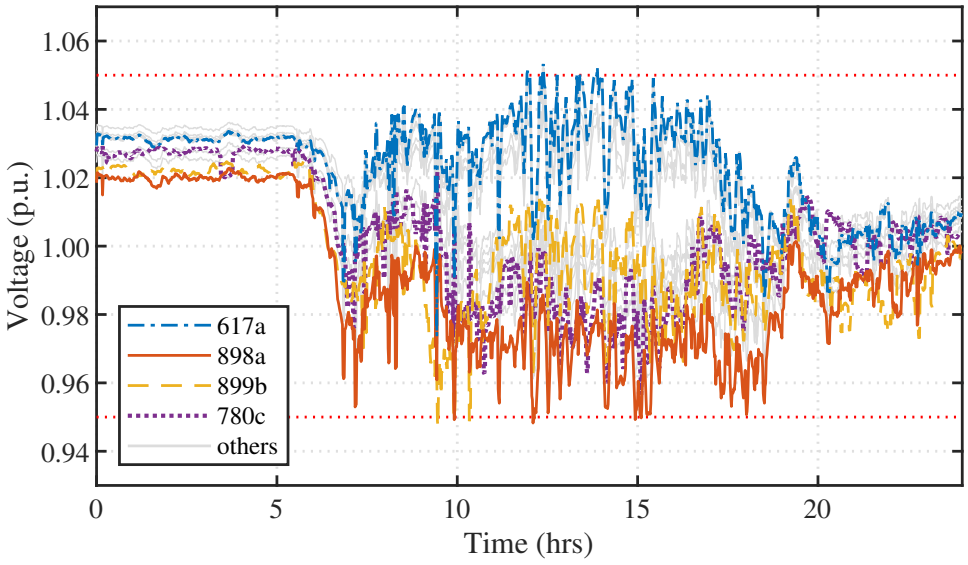

(b)

Figure 2.17: Voltage profiles of the network over a 24-hour period. (a) Without PV reactive power compensation; (b) With the proposed strategy.

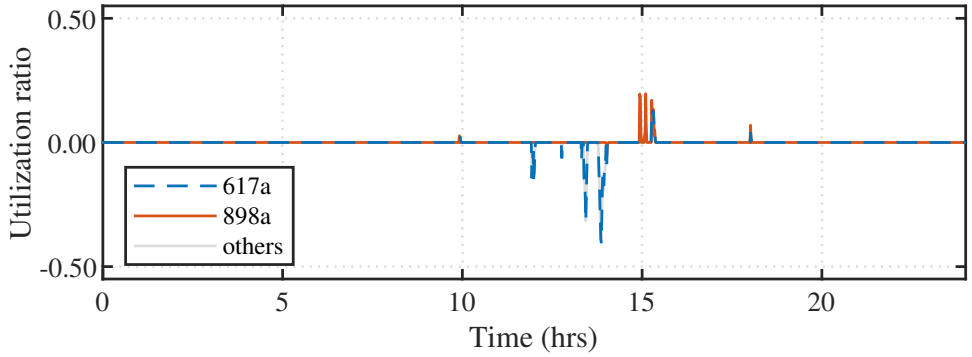

(a)

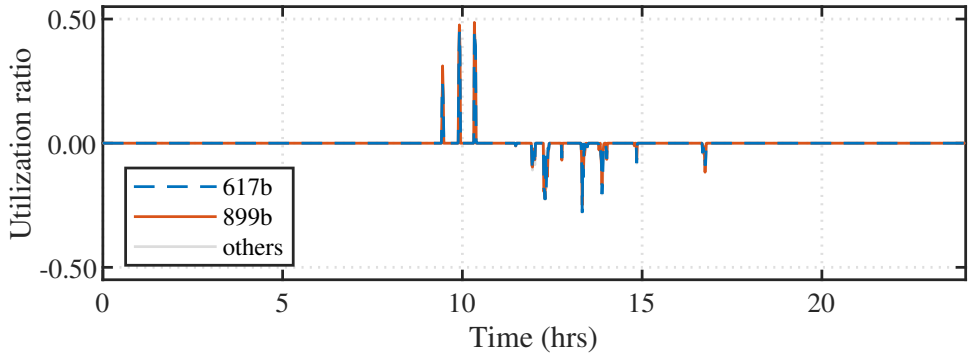

(b)

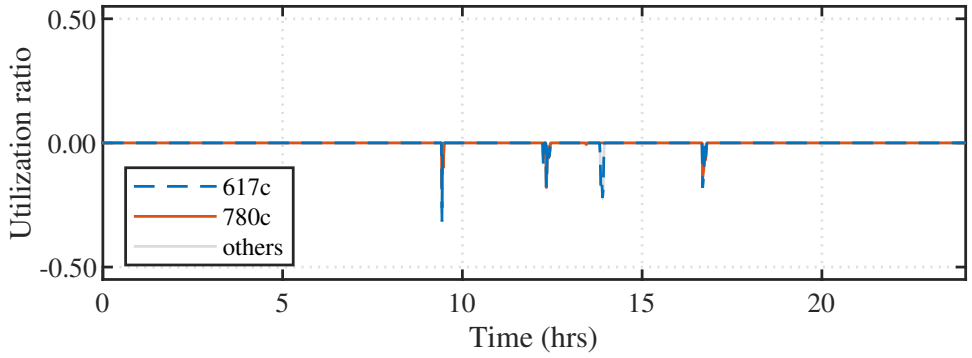

(c)

Figure 2.18: Utilization ratios of the smart PV inverter over a 24-hour period. (a) Phase a; (b) Phase b; (c) Phase c.

2.8 Summary

This chapter developed and demonstrated a dynamic distributed control strategy to form coalition of PV inverters and their coordinated control for voltage regulation in distribution networks. This strategy is required when uneven integration of PV capacity creates large voltage differences along a feeder. On the slower time-scale, the coalition formation scheme separates opposing voltage violation problems and assigns them to groups of inverters with similar voltage margins and sufficient regulation capacity. On the faster time-scale, the feedback-based leader-follower consensus algorithm guides PV inverters within each coalition to eliminate the voltage violations while reaching a consensus on their utilization ratios. This control strategy effectively maintains voltages within the acceptable range while ensuring a sufficient and fair utilization of the available voltage regulation resources.

Chapter 3

BI-LEVEL VOLT/VAR OPTIMIZATION IN DISTRIBUTION NETWORKS WITH SMART PV INVERTERS

Optimal Volt/VAR control (VVC) in distribution networks relies on the effective coordination between the conventional utility-owned mechanical devices and the smart residential photovoltaic (PV) inverters. Typically, a central controller carries out a periodic optimization and sends setpoints to the local controller of each device. However, instead of tracking centrally dispatched setpoints, smart PV inverters can cooperate on a much faster timescale to reach optimality within the PV inverter group. To accommodate such a PV inverter group in the VVC architecture, this chapter proposes a bi-level optimization-based framework. The upper-level determines the setpoints of the mechanical devices to minimize the network active power losses, while the lower-level represents the coordinated actions that the inverters take for their own objectives. The interactions between these two levels are captured in the bi-level optimization model, which is solved based on the Karush-Kuhn-Tucker (KKT) conditions. This framework fully exploits the capabilities of the different types of voltage regulation devices and enables them to cooperatively optimize their goals. Case studies on a typical distribution network with field-recorded data demonstrate the effectiveness and advantages of the proposed approach.

3.1 Introduction

Volt/VAR control (VVC) manages voltage levels and reactive power in distribution networks to reduce active power losses and maintain acceptable voltage magnitudes using on-load tap changers (OLTCs) and capacitor banks (CBs) [51]. However, the high penetration of residential rooftop photovoltaic (PV) generation has caused rapid voltage fluctuations that these conventional mechanical devices are not designed to handle [6, 7]. On the other hand, smart PV inverters with sensing, communicating and computing capabilities are able to act autonomously to provide fast and flexible reactive power compensation for voltage regulation [11]. They are thus encouraged to participate in VVC by the IEEE 1547 Standard [18].

This chapter develops a bi-level optimization framework for the VVC in distribution networks. The upper-level optimization determines the periodic dispatch of the slower mechanical devices to minimize the network active power losses. It is formulated as a mixed integer second order cone programming (MISOCP) model that contains a nested lower-level optimization as the constraint on PV inverter reactive output. This optimization problem is intended to be centrally solved in an Advanced Distribution Management System (ADMS) based on the network information after replacing the lower-level with its Karush-Kuhn-Tucker (KKT) conditions. The lower-level optimization takes the settings of OLTCs and CBs as input parameters and models the coordinated outputs of the smart PV inverters. These inverters remove sudden voltage limit violations between upper-level dispatch periods while optimizing their group objectives, e.g. minimizing the reactive power cost or equitably sharing the reactive power contributions for voltage regulation. The lower-level optimization is solved in a distributed manner as the PV inverters adjust their outputs autonomously based on real-time voltage measurement and neighboring communication.

3.1.1 Literature Review

Various strategies have been proposed for the coordinated voltage regulation in distribution networks. Based on the autonomy level of the inverters, they can be broadly classified into

three categories.

Strategies of the first category periodically optimize the setpoints and send them to the local controller of each device, which implements these setpoints directly. The autonomous VVC control capability of the smart inverters is thus not fully exploited. For example, Jha et al. [52] solve a mixed integer linear programming (MILP) problem to set the CBs and OLTCs. While the inverters are dispatched based on the solution of a nonlinear programming (NLP) problem that more accurately models the power flows. To accelerate the optimization and maintain customer data privacy, the modified alternating direction method of multipliers (ADMM) that can handle discrete variables is used in [53, 54] to solve the VVC optimization problem. Two-stage stochastic optimization [55] and robust optimization [56] algorithms have been implemented to handle uncertainty on the renewable generation in the optimal reactive power dispatch. These control strategies are open-loop and implement feedforward optimization techniques which rely on the network information and forecasts. They are generally less robust to model and forecast errors and also less effective in dealing with fast voltage fluctuations [57].

In the second category of strategies, the smart PV inverters follow the centrally-optimized setpoints while they also adjust their reactive output based on real-time local measurements to improve the control performance. In [58], the inverter generates the reactive power dispatched by the central controller when its local voltage is within the allowable operational limits, otherwise the droop control is activated. Malekpour et al. further added a distributed algorithm to allocate the voltage regulation burden among inverters in proportion to their capacities [59]. Besides the reactive power setpoint, inverters can also be controlled to track the voltage references [60]. Instead of just considering the upper and lower reactive power limits of the inverters, several authors [61, 62, 63] model their reactive power generation as a function of the local voltage in the optimization model, which allows the central controller to also optimize the local droop control parameters for the PV inverter. These multi-level control strategies combine the system-wide feedforward optimization with the real-time local feedback control to increase robustness to forecast errors and fast fluctuations in renewable

generation. However, the local linear droop control in [58, 60, 61, 62, 63] may fail to maintain the real-time voltage within the acceptable range when the locally available reactive power is insufficient [64]. The reactive power capacity of the whole system is utilized in [59], while its reactive power reallocation can cause a large deviation between the actual inverter output and the optimized setpoint and affect the optimality of the VVC strategy.

The third category of strategies emerged recently with the development of smart inverter technology. These inverters continuously and autonomously adjust their output while cooperating with each other through neighboring communication. Strategies in [24, 25] implement the leader-follower consensus algorithm, which enables the smart inverters to regulate the network voltage magnitude while sharing the regulation burden according to their maximum available capacity. Other strategies rely on the distributed optimization methodology, such as dual ascent algorithm [64, 65, 66, 21] and primal-dual gradient algorithm [22]. By emulating the iterative steps of these algorithms, the PV inverter group achieves optimal coordination in real-time to remove local voltage violations while minimizing power losses [64, 65, 66], reactive power cost [21] or a weighted sum of them both [22]. These strategies fully exploit the flexibility and fast response capability of smart PV inverters. Moreover, they do not need to model the variations of load or renewable generation explicitly, instead, the smart PV inverters adjust their output by constantly monitoring the dynamic system. Such feedback optimization-based strategies are more robust to model error and uncertainty in renewable generation, and they can also improve the dynamic performance of the closed-loop system [57]. However, the slower mechanical devices with discrete control actions are unable to participate in such strategies and they still rely on the central controller. As the PV inverters gain more autonomy, their interactions with the centrally controlled mechanical devices need to be handled more carefully. Otherwise, unnecessary control actions or even operational conflicts might occur [67]. Furthermore, because they are owned by the consumers, the VVC objective of the PV inverters can be different from that of the utility's. Assuming PV inverters track the setpoint from the utility and simply modelling its reactive output as box or quadratic constraint while optimizing the mechanical devices becomes less

valid. A new frameworks is needed to effectively incorporate the smart PV inverter in VVC.

3.1.2 Contribution

The main contributions of this chapter are:

- A bi-level optimization model which captures the interactions between the utility and consumer-owned devices. The upper-level contains the lower-level as a constraint, which reflects that the residential PV inverters' reactive output would influence the network active power losses. On the other hand, the lower-level takes the upper-level determined OLTC and CB settings as parameters, as those values would in turn impact the local voltage magnitude of the PV inverters.

- A solution based on the KKT conditions that guarantees an optimal control of both the mechanical devices and the PV inverters. The upper-level becomes a solvable MISOCP model after replacing the lower-level with its KKT conditions. The ADMS solves this problem to optimally schedule the mechanical devices while taking account of the PV inverters' response. The smart PV inverters emulates the KKT condition-based distributed optimization algorithms to adjust their reactive output with local voltage measurement, which iteratively solves the lower-level optimization under the upper-level determined OLTC and CB settings.

- A two-timescale VVC framework which combines the advantages of feedforward and feedback optimizations. The upper-level deals with the slower voltage variations caused by regular daily variations in load and PV generation. It makes use of the available network information in the ADMS to achieve a system-wide optimal coordination. On the real-time scale, the fast and autonomous PV inverters cooperate to remove the instantaneous voltage violations, which improves the dynamic voltage control performance and the robustness of the framework.

3.1.3 Chapter Organization

The remainder of this chapter is organized as follows. Section 3.2 describes the details of the bi-level optimization model. Section 3.3 presents the solution approach and its implementation. Section 3.4 demonstrates and analyzes simulation results. Section 3.5 summarizes and concludes.

3.2 Bi-level Optimization Model

This section describes the objectives and constraints of the upper and lower-level optimization models. The composite bi-level optimization model is then presented.

3.2.1 Upper-level

The upper-level dispatches OLTCs and CBs to minimize the network active power losses over the time horizon $\{1, ..., t_H\}$:

$$F = \sum_{t=1}^{t_H} \sum_{(i,j)\in\mathcal{E}} r_{ij} l_{ij,t}. \tag{3.1}$$

Meanwhile, it must satisfy the following constraints $\forall i \in \mathcal{N}$, $\forall (i,j) \in \mathcal{E}$, $\forall t \in \{1, ..., t_H\}$.

a) System Operational Constraints: The DistFlow model proposed in [68] has been extensively used for modeling distribution networks because of its accuracy and computational efficiency. It formulates the power flow constraints as follows:

$$P_{ij,t} = \sum_{k:(j,k)\in\mathcal{E}} P_{jk,t} + r_{ij} l_{ij,t} + \hat{p}^l_{j,t} - \hat{p}^g_{j,t} \tag{3.2}$$

$$Q_{ij,t} = \sum_{k:(j,k)\in\mathcal{E}} Q_{jk,t} + x_{ij} l_{ij,t} + \hat{q}^l_{j,t} - q^g_{j,t} - q^c_{j,t} \tag{3.3}$$

$$v_{j,t} = v_{i,t} - 2(r_{ij} P_{ij,t} + x_{ij} Q_{ij,t}) + (r^2_{ij} + x^2_{ij}) l_{ij,t} \tag{3.4}$$

$$l_{ij,t} v_{i,t} = P^2_{ij,t} + Q^2_{ij,t} \tag{3.5}$$

Since the equality constraint (3.5) is non-convex, we relax it to an inequality constraint using the method proposed in [46] to obtain a global optimal solution:

$$\left\| \begin{bmatrix} 2P_{ij,t} & 2Q_{ij,t} & l_{ij,t} - v_{i,t} \end{bmatrix}^T \right\|_2 \leq l_{ij,t} + v_{i,t}. \tag{3.6}$$

On the primary and secondary sides of an OLTC, (3.4) is modified as follows:

$$\frac{v_{j,t}}{T_{ij,t}} = v_{i,t} - 2(r_{ij}P_{ij,t} + x_{ij}Q_{ij,t}) + (r_{ij}^2 + x_{ij}^2)l_{ij,t} \tag{3.7}$$

where T_{ij} is the squared turns ratio. For each tap position $n \in \{1, ..., N_{ij}^T\}$, there is a corresponding T_{ij}^n. Thus,

$$\frac{1}{T_{ij,t}} = \sum_{n=1}^{N_{ij}^T} \frac{w_{ij,t}^n}{T_{ij}^n} \tag{3.8}$$

where

$$\sum_{n=1}^{N_{ij}^T} w_{ij,t}^n = 1, \quad w_{ij,t}^n \in \{0, 1\}, \tag{3.9}$$

i.e. only one of the auxiliary binary variables $w_{ij,t}^n$ is nonzero, which specifies the selection of one turns ratio. Moreover, the nodal voltages and branch currents must be maintained within the acceptable range:

$$\underline{v}_i \leq v_{i,t} \leq \bar{v}_i, \tag{3.10}$$

$$l_{ij,t} \leq \bar{l}_{ij}. \tag{3.11}$$

b) Control Devices Operational Constraints: The tap change between two dispatch periods, as well as the total tap change of the OLTC during the whole dispatch horizon should be limited to reduce mechanical wear and tear:

$$|n_{ij,t}^T - n_{ij,t-1}^T| \leq \Delta\bar{n}_{ij}^T \tag{3.12}$$

$$\sum_{t=1}^{t_H} |n_{ij,t}^T - n_{ij,t-1}^T| \leq \bar{n}_{ij}^T \tag{3.13}$$

$$n_{ij,t}^T \in \{1, ..., N_{ij}^T\}. \tag{3.14}$$

Similarly, the operational constraints for CBs are:

$$|n_{i,t}^C - n_{i,t-1}^C| \leq \Delta \bar{n}_i^C \tag{3.15}$$

$$\sum_{t=1}^{t_H} |n_{i,t}^C - n_{i,t-1}^C| \leq \bar{n}_i^C \tag{3.16}$$

$$n_{i,t}^C \in \{0, ..., N_i^C\}. \tag{3.17}$$

The reactive power injection from CBs is

$$q_{i,t}^c = \frac{n_{i,t}^C}{N_i^C} Q_i^C. \tag{3.18}$$

The equality constraint on the PV inverters reactive output is a nested optimization problem corresponding to their coordinated autonomous operation:

$$\mathbf{q}_t^g \in \arg\min_{\mathbf{q}_t^g} \{f(\mathbf{q}_t^g) : \mathbf{G} \leq 0\} \tag{3.19}$$

where $\mathbf{q}_t^g$ is the vector containing $q_{i,t}^g$, $\forall i \in \mathcal{N}_\mathcal{G}$. $f(\mathbf{q}_t^g)$ and $\mathbf{G}$ are the objective function and set of constraints of the lower-level optimization, which are detailed in the next subsection.

3.2.2 Lower-level

In the lower-level, the PV inverters cooperate to achieve an optimal utilization of their reactive power while removing instantaneous voltage limit violations:

$$\begin{aligned} \min_{\mathbf{q}_t^g} \quad & f(\mathbf{q}_t^g) \\ \text{s.t.} \quad & \underline{v} \leq v_{i,t} \leq \bar{v}, \ \forall i \in \mathcal{N}_\mathcal{G} \\ & \underline{q}_{i,t} \leq q_{i,t}^g \leq \bar{q}_{i,t}, \ \forall i \in \mathcal{N}_\mathcal{G} \end{aligned} \tag{3.20}$$

where $\bar{q}_{i,t}$ and $\underline{q}_{i,t}$ are the upper and lower PV inverter reactive output limits, $\bar{q}_{i,t} = \sqrt{(s_i^g)^2 - (p_{i,t}^g)^2}$ and $\underline{q}_{i,t} = -\bar{q}_{i,t}$. Different objective functions can be set:

a) Minimize Reactive Power Cost: The provision of reactive power for VVC normally requires excess capacity on the inverters, and thus over-sizing hardware design or active power

curtailment. The PV inverters could seek to minimize their reactive power cost [21, 22]:

$$f(\mathbf{q}_t^g) = \sum_{i \in \mathcal{N}_\mathcal{G}} a_i^2 (q_{i,t}^g)^2 + b_i (q_{i,t}^g) + c_i \tag{3.21}$$

where a_i, b_i, c_i are synthetic cost parameters.

b) Minimize Network Active Power Losses: The PV inverter group could also minimize the network active power losses associated with their reactive output. For ease of implementation, the objective function is usually defined as [64, 65]:

$$f(\mathbf{q}_t^g) = (\mathbf{q}_t^g)^T X_{gg} (\mathbf{q}_t^g) \tag{3.22}$$

where X_{gg} is a submatrix of X, whose elements are:

$$X_{ij} := 2 \sum_{(h,k) \in \mathcal{P}_i \cap \mathcal{P}_j} x_{hk} \tag{3.23}$$

where $\mathcal{P}_i$ is the set of distribution lines on the unique path from the substation to bus i. Partition X based on $i \in \mathcal{N}_\mathcal{G}$ or $i \notin \mathcal{N}_\mathcal{G}$:

$$X = \begin{bmatrix} X_{gg} & X_{gl} \\ X_{lg} & X_{ll} \end{bmatrix}. \tag{3.24}$$

X_{gg} is the submatrix associated with the PV nodes and it is a positive definite matrix [64, 22]. Besides, this objective function also promotes uniform voltage drops [64].

c) Equalize Utilization Ratios: The utilization ratio of an inverter in the VVC is the proportion of its maximum available reactive power capacity used for voltage regulation, i.e., $u_i = q_i^g / \bar{q}_i$. To prevent excessive use and early saturation of certain inverters, the PV inverter group could cooperate to generate at the same utilization ratio. The leader inverter, typically the inverter at the end node as it usually experiences the largest voltage deviation, measures its local voltage to determine the utilization ratio [24, 25]. The lower-level optimization objective can be formulated as:

$$f(\mathbf{q}_t^g) = \sum_{i \in \mathcal{N}_\mathcal{G}} \frac{X_{li}}{2\bar{q}_{i,t}} (q_{i,t}^g)^2 \tag{3.25}$$

where $l \in \mathcal{N}_{\mathcal{G}}$ is the index of the leader inverter. The proof is detailed in the Appendix.

Moreover, $f(\mathbf{q}_t^g)$ can also be defined as a weighted sum of these objectives. For example, the PV inverter objective function in [22] combines (3.21) and (3.22). For a network that contains several groups of PV inverters located in different control zones and where there is no inter-group coordination, the lower-level can be modified into a set of two or more optimization models. Each of these models describes the coordinated action of a PV inverter group.

3.2.3 Bi-level Optimization Model

The bi-level optimization can be summarized as follows:

$$\begin{aligned} \min_{n_{ij,t}^T,\, n_{i,t}^C} \quad & F \\ \text{s.t.} \quad & (3.2)-(3.4),\ (3.6)-(3.18), \\ & \mathbf{q}_t^g \in \arg\min_{\mathbf{q}_t^g} \Big\{ f(\mathbf{q}_t^g) : \underline{v} \le v_{i,t} \le \bar{v}, \\ & \qquad\qquad \underline{q}_{i,t} \le q_{i,t}^g \le \bar{q}_{i,t},\ \forall i \in \mathcal{N}_{\mathcal{G}} \Big\} \end{aligned} \tag{3.26}$$

Each of the two optimization tasks has its own objective, constraints and decision variables. The two levels are coupled because the active network losses depend on the PV inverter reactive output and the PV inverters' local voltage magnitude is influenced by the settings of the mechanical devices. This bi-level optimization model is an extension of the traditional single-level model. It reduces to the single-level model if we remove the lower-level objective function and make $\mathbf{q}_t^g$ an upper-level decision variable. This bi-level extension is necessary to effectively utilize the reactive power from the PV inverters for system-wide VVC while fully exploiting their autonomous real-time VVC capability.

3.3 Solution Approach and Implementation

This section describes the solution approach and the implementation of the bi-level optimization model. The key idea involves representing the lower-level optimization by its KKT

conditions. The ADMS and the smart PV inverters operate to ensure these conditions are satisfied in their own ways.

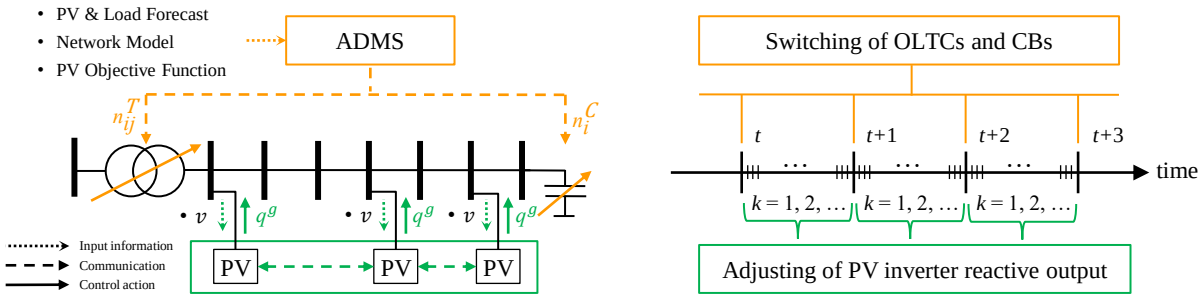

Figure 3.1: Overview of the implementation of the bi-level optimization model.

3.3.1 KKT Conditions

With objective function (3.21), (3.22) or (3.25), the lower-level optimization problem (3.20) is convex. Assume the Slater condition is satisfied, i.e. there exist $\underline{q}_i < q^g_{i,t} < \bar{q}_i$, $\forall i \in \mathcal{N}_\mathcal{G}$ such that $\underline{v} < v_{i,t} < \bar{v}$, $\forall i \in \mathcal{N}_\mathcal{G}$, then this problem can be replaced by its KKT conditions:

$$\begin{aligned}\nabla_{q^g_{i,t}} \Big\{ f(\mathbf{q}^g_t) + \sum_{i\in\mathcal{N}_\mathcal{G}} \underline{\lambda}_{i,t}(\underline{v} - v_{i,t}) + \sum_{i\in\mathcal{N}_\mathcal{G}} \bar{\lambda}_{i,t}(v_{i,t} - \bar{v}) \\ + \sum_{i\in\mathcal{N}_\mathcal{G}} \underline{\mu}_{i,t}(\underline{q}_{i,t} - q^g_{i,t}) + \sum_{i\in\mathcal{N}_\mathcal{G}} \bar{\mu}_{i,t}(q^g_{i,t} - \bar{q}_{i,t}) \Big\} = 0\end{aligned} \tag{3.27}$$

$$\underline{v} \le v_{i,t} \le \bar{v}, \quad \underline{q}_{i,t} \le q^g_{i,t} \le \bar{q}_{i,t} \tag{3.28}$$

$$\underline{\lambda}_{i,t}(\underline{v} - v_{i,t}) = 0, \quad \bar{\lambda}_{i,t}(v_{i,t} - \bar{v}) = 0 \tag{3.29}$$

$$\underline{\mu}_{i,t}(\underline{q}_{i,t} - q^g_{i,t}) = 0, \quad \bar{\mu}_{i,t}(q^g_{i,t} - \bar{q}_{i,t}) = 0 \tag{3.30}$$

$$\underline{\lambda}_{i,t},\ \bar{\lambda}_{i,t},\ \underline{\mu}_{i,t},\ \bar{\mu}_{i,t} \ge 0 \tag{3.31}$$

$\forall i \in \mathcal{N}_\mathcal{G}$. In which, $\underline{\lambda}_{i,t}$, $\bar{\lambda}_{i,t}$, $\underline{\mu}_{i,t}$, $\bar{\mu}_{i,t}$ are dual variables.

3.3.2 Control of OLTCs and CBs

As Fig. 3.1 shows, The ADMS dispatches OLTCs and CBs based on a full knowledge of the network, which includes forecast of the load and PV generation, network model, as well as the objective function selected by the PV owners. For each dispatch horizon, it constructs the bi-level optimization model described in Section II and then takes the single-level reduction approach [69] to replace the lower-level with its KKT conditions. The sensitivity of the squared voltage to the inverter reactive output $\partial v_{i,t}/\partial q^g_{j,t}$ in (3.27) can be approximated by X_{ij} [70] or calculated based on the Jacobian matrix. The bi-linear constraint stemming from the complementary slackness condition can be handled using the big-M method, which replaces Eqs. (3.29)-(3.30) by:

$$\underline{\lambda}_{i,t} \le M\underline{\sigma}_{i,t}, \quad v_{i,t} - \underline{v} \le M(1-\underline{\sigma}_{i,t}) \tag{3.32}$$

$$\bar{\lambda}_{i,t} \le M\bar{\sigma}_{i,t}, \quad \bar{v} - v_{i,t} \le M(1-\bar{\sigma}_{i,t}) \tag{3.33}$$

$$\underline{\mu}_{i,t} \le M\underline{\delta}_{i,t}, \quad q^g_{i,t} - \underline{q}_{i,t} \le M(1-\underline{\delta}_{i,t}) \tag{3.34}$$

$$\bar{\mu}_{i,t} \le M\bar{\delta}_{i,t}, \quad \bar{q}_{i,t} - q^g_{i,t} \le M(1-\bar{\delta}_{i,t}) \tag{3.35}$$

$\forall i \in \mathcal{N}_\mathcal{G}$, where M is a large number, $\underline{\sigma}_{i,t}$, $\bar{\sigma}_{i,t}$, $\underline{\delta}_{i,t}$, $\bar{\delta}_{i,t}$ are auxiliary binary variables. Consequently, the bi-level optimization problem becomes a solvable single-level MISOCP problem:

$$\begin{aligned} \min_{n^T_{ij,t}, n^C_{i,t}, \mathbf{q}^g_t, \underline{\lambda}_{i,t}, \bar{\lambda}_{i,t}, \underline{\mu}_{i,t}, \bar{\mu}_{i,t}} \quad & F \\ \text{s.t.} \quad (3.2)-(3.4),\ (3.6)-(3.18), (3.27),\ (3.28),\ (3.31)-(3.35). & \end{aligned} \tag{3.36}$$

The ADMS can solve this problem using off-the-shelf optimization tools. At each dispatch period t, it delivers the setpoints to the local controllers of OLTCs and CBs via the supervisory control and data acquisition (SCADA) system or the communication link between the devices and ADMS. These setpoints are then implemented and kept unchanged until the next dispatch period $t+1$.

3.3.3 Control of PV Inverters

The PV inverters cooperate to solve the lower-level optimization problem autonomously. While individual inverters do not have access to global information about the system, they are able to take rapid control actions by measuring their local voltage magnitude and exchanging information with other inverters via Wi-Fi, ZigBee or power line communication (PLC). These capabilities enable them to iteratively adjust their output towards the satisfaction of the KKT conditions by implementing fully-distributed control strategies [64, 66, 21, 22]. These strategies are of different design, for example, the strategy proposed in [64] adds an additional feedback loop to deal with the reactive power constraint, while this constraint is handled by a special quadratic penalty function in [22]. [66] focuses on the limited bandwidth of the communication link, whereas [66] addresses the delayed communication. However, the execution of these strategies are similar. As Fig. 3.1 shows, at each iteration cycle $k \in [t, t+1]$, a inverter performs the following four major steps:

- Measure the local voltage magnitude;
- Calculate the control signal based on pre-defined logic;
- Implement the control signal to adjust reactive output;
- Exchange information with neighbors.

This four-step action is similar to one iteration step in the dual ascent or primal-dual gradient algorithms. As these algorithms solve the lower-level optimization problem iteratively, the inverter output converges to the optimal value asymptotically. The detailed strategies and theoretical proof of convergence and optimality can be found in [64, 66, 21, 22]. Moreover, the practicability of the feedback optimization-based strategy, such as its robustness against measurement noise, real-time computational feasibility, effectiveness under asynchronous communication, etc., has been validated by field test results in the real distribution network [70].

3.3.4 Discussion

In the implementation, the ADMS follows the feedforward optimization process. It models the coordinated actions of the PV inverters based on a full knowledge of the network and is thus able to influence those actions indirectly via changing the PV inverters' local voltage magnitude using the OLTCs and CBs. In this way, the ADMS exploits the reactive power compensation capability of PV inverters for system-wide optimal VVC while respecting their autonomy. On the other hand, the feedback optimization-based lower-level solution approach enables the PV inverters to take actions based on the constant monitoring of their local voltage. The switching of the mechanical devices are essentially taken into consideration when they optimize their goals.

3.4 Case Studies

3.4.1 Test System

Fig. 3.2 shows the single-line diagram of the balanced IEEE 33-bus radial distribution network [68] used to demonstrate the performance of the proposed VVC framework. The green dashed lines represent the communication links between neighboring inverters. The nonlinear AC power flow model of the test system was constructed using MATPOWER [45]. Table 3.1 shows the capacities of the 12 aggregated residential PV systems. The peak load is assumed to be 1.25 times the load value in [68]. The 1-minute-resolution daily profiles for PV generation and load consumption was constructed based on the Pecan Street data set of June 16, 2014 [43]. The hourly PV and load forecast value used by the ADMS are their hourly average value with a random percent error, $\pm 20\%$ for PV generation and $\pm 10\%$ for load consumption. Fig. 3.3 shows their normalized profiles and forecast values over the course of one day. Each PV inverter is oversized by 10% so it can provide reactive power compensation while generating at its rated active power capacity [18]. An OLTC allows for ± 0.05 p.u. voltage regulation connects the network with the substation. Each of its 17 tap positions, labeled as $\{-8, -7, ..., -1, 0, 1, ..., 7, 8\}$, provides 0.00625 p.u. regulation. 3 identical CBs are installed

at nodes 6, 16 and 24. The acceptable voltage range is 0.95 p.u. to 1.05 p.u. The upper-level optimizes over a 3-hour horizon and sends hourly setpoint to the OLTC and CBs. The PV inverter objective function in the lower-level is $f(\mathbf{q}_t^g) = a_i^2(q_{i,t}^g)^2 + (\mathbf{q}_t^g)^T X_{gg}(\mathbf{q}_t^g)$ where a_i is a synthetic value in the range of $[0.5, 1.5]$. The PV inverters implement the strategy proposed in [22] to adjust their output every 0.5 seconds. Table 3.2 summarizes the rest operational parameters of the mechanical devices.

Fig. 3.4 shows the voltage profiles of the network when no control strategy is implemented. Due to the fast fluctuation in load and PV generation, the voltage magnitude changes rapidly. Moreover, the system experiences over-voltage issues at mid-day, when the high PV generation exceeds the local load and causes reverse power flow. On the other hand, after 19:00, the heavy load leads to under-voltage problems.

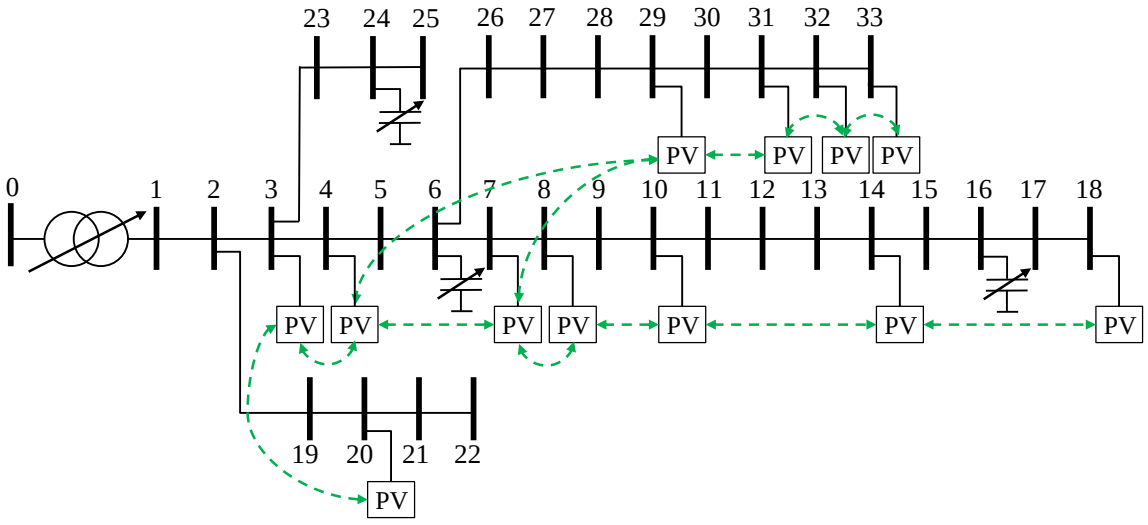

Figure 3.2: Single-line diagram of the test system.

3.4.2 Results and Analysis

Fig. 3.5 shows the voltage regulation results with our proposed optimal VVC. Over the course of the day, all the voltage regulation devices cooperate together and effectively constrain the

Table 3.1: Capacities of the PV Systems

Capacity (kW)	200	220	240	250	300	450	600	650
Node	3, 20	7	18	33	4, 8, 10	14	32	29, 31

Table 3.2: Parameters of the Mechanical Devices

$\Delta\bar{n}_i^C$	$\bar{n}_i^C$	$\Delta\bar{n}_{ij}^T$	$\bar{n}_{ij}^T$	N_i^C	Q_i^C (kVAr)
1	2	2	5	3	300

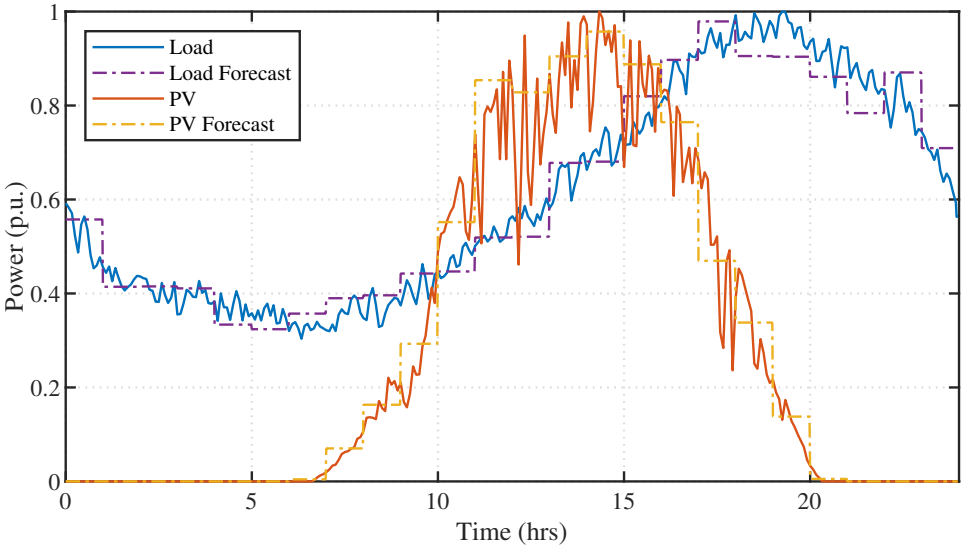

Figure 3.3: Normalized daily profiles and forecast of PV and load.

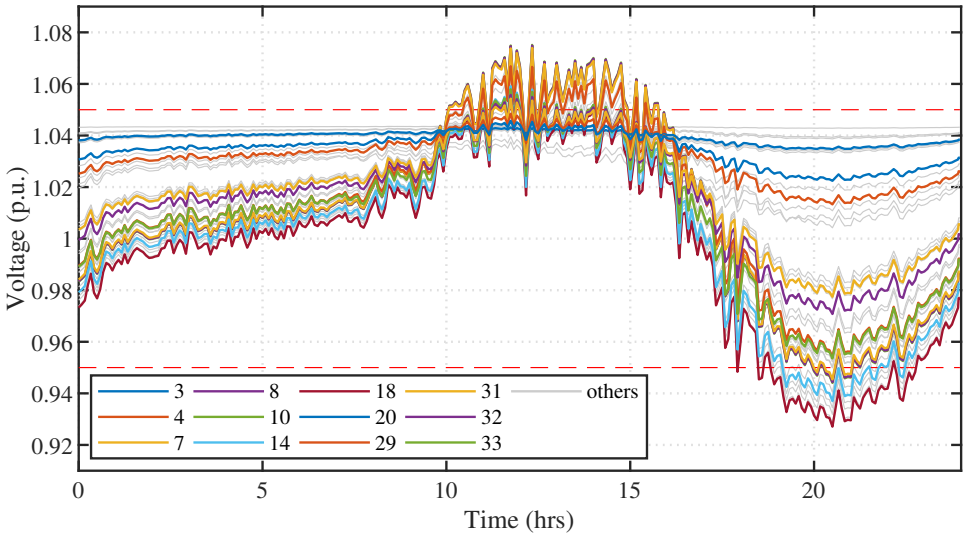

Figure 3.4: Network voltage profiles without any control.

voltage profiles within the specified range. Moreover, the average daily active power loss across the network is reduced by 22.48%, from 101.26 kW to 78.50 kW.

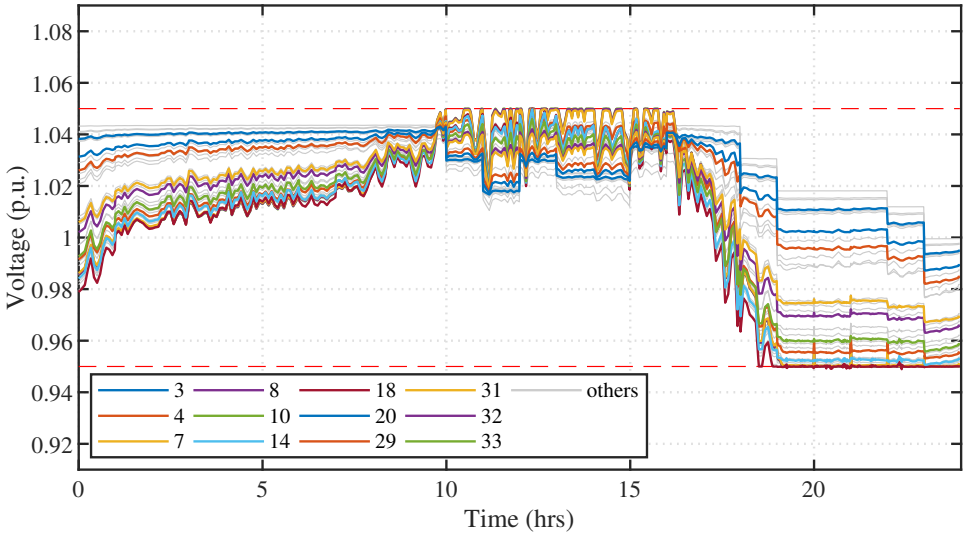

Figure 3.5: Network voltage profiles with the proposed control.

Fig. 3.6 shows the switching actions of the mechanical devices and Fig. 3.7 illustrates the

PV inverter reactive power output. Before 19:00, the ADMS adjusts the OLTC tap position and the number of CB units to maintain a relatively high voltage level across the network so as to reduce the active power losses. During this period, since the ADMS only updates the setpoints of the OLTC and CBs on an hourly basis and forecast errors arise, voltage limit violations occur within the dispatch period. When the fast-reacting PV inverters detect these violations, they cooperate to remove them at the minimal value of their group objective. For example, the rapid increase in active PV generation leads to an instant over-voltage problem at 11:53. In response, the PV inverters absorb reactive power to lower the voltage. Moreover, as shown in Fig. 3.8, the reactive power outputs of the PV inverters (solid lines) converge to the optimal solution of problem (3.20) (dashed lines) within about 30 seconds, thereby illustrating their ability to solve the lower-level optimization problem cooperatively. After 19:00, however, the ADMS determines that it can minimize the upper-level optimization objective by forcing the PV inverters to provide reactive power to mitigate the loading of the distribution lines. Therefore, the ADMS switches down the mechanical devices and deliberately sets the voltage magnitude of node 18 at the lower voltage limit. As a result, the PV inverter group maintains a constant reactive power provision to the network, which alleviates the loading of the distribution network and reduces the active power losses. This reactive power varies in response to the fast fluctuations of the load consumption and the switching of the mechanical devices.

3.4.3 Comparison with other Approaches

The proposed bi-level optimization model is necessary to accommodate the coordinated actions of the PV inverters in the VVC architecture. We demonstrate this by comparing the above simulation results with two other approaches where the PV inverters still implement the strategy proposed in [22] but the OLTC and CBs are dispatched using two traditional single-level optimization models. These two models are obtained by removing the lower-level objective function from the bi-level model and treating the PV inverter reactive power outputs in two ways:

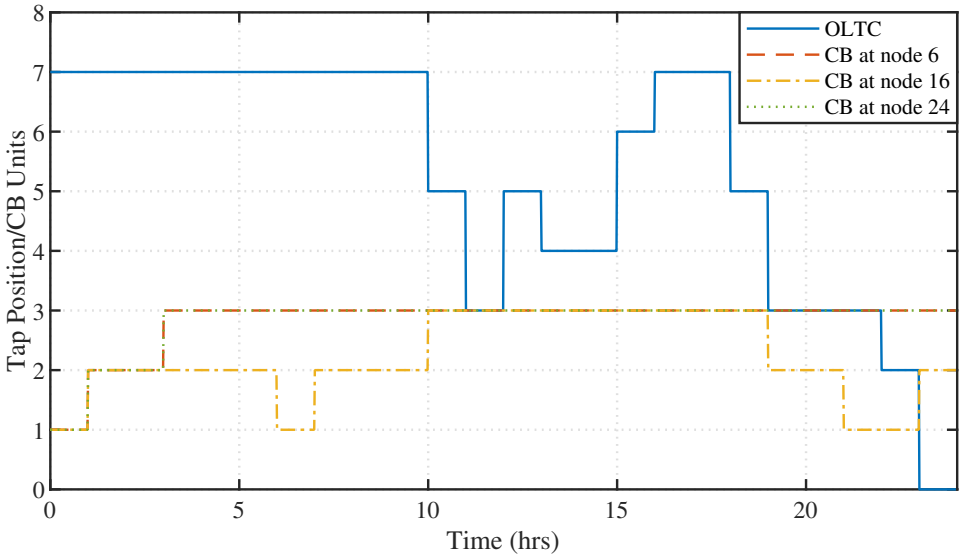

Figure 3.6: Switching actions of the mechanical devices.

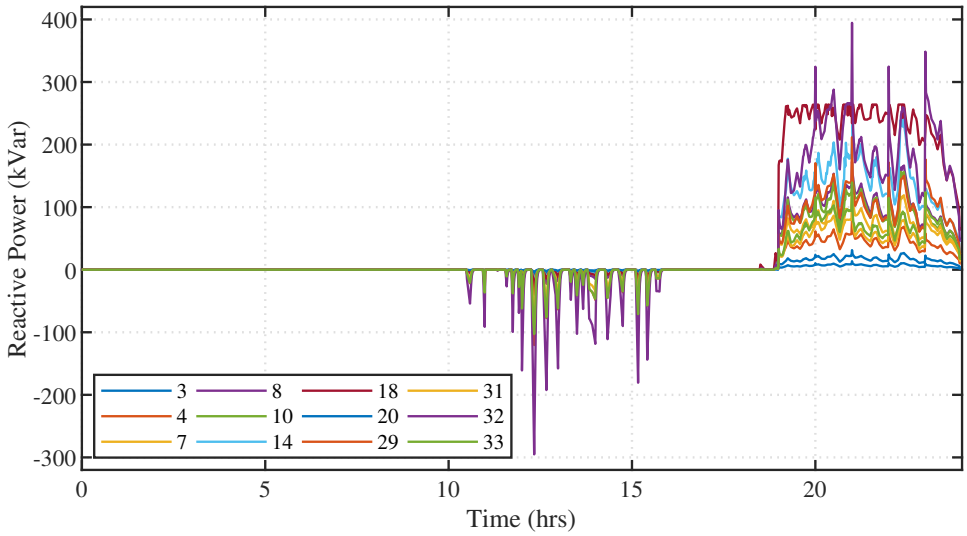

Figure 3.7: PV inverter reactive power output.

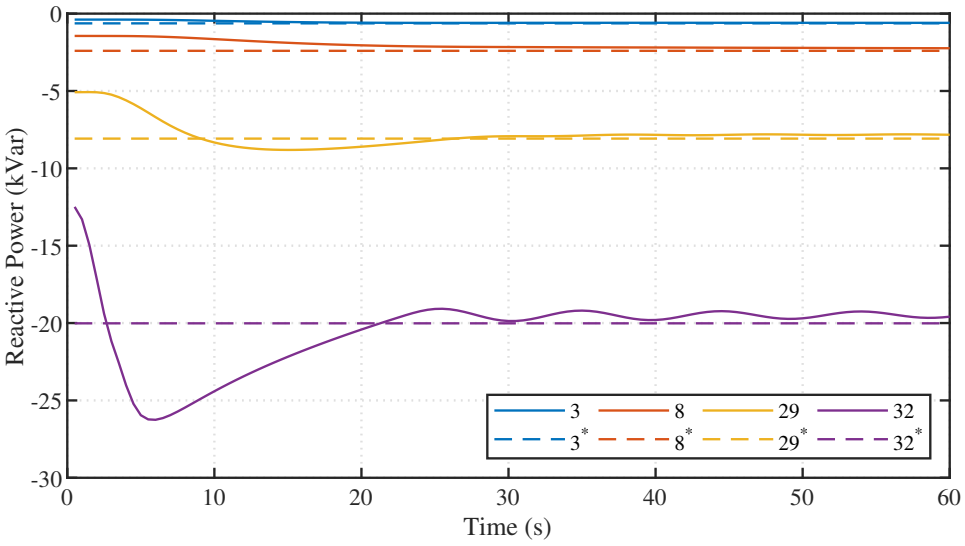

Figure 3.8: PV inverter reactive output iteration process at 11:53.

- Model 1: Assume the PV inverters follow the centrally-dispatched setpoints and include $\mathbf{q}_t^g$ as a decision variable;

- Model 2: Ignore the PV inverter reactive power output and remove $\mathbf{q}_t^g$ from the optimization model.

We compare these models based on the theoretical power loss obtained by solving the optimization problem and based on the actual power loss observed after implementing the optimized switching plans for the OLTC and CBs. Table 3.3 shows the theoretical and actual average daily active power loss P^*_{loss} and P_{loss}. Fig. 3.9 and Fig. 3.10 show these profiles over the 24-h simulation period. For the theoretical power loss, since Model 1 assumes that the PV inverters are directly controllable, it achieves the minimum value. On the other hand, as Model 2 does not use the PV inverters at all, the resulting loss is thus the highest. Our proposed model does not assume the PV inverters can be directly controlled, while it allows the ADMS to indirectly influence their reactive output when necessary. Hence it achieves a medium level power loss result. However, when it comes to the actual power loss,

Model 1 results in the highest value among the three cases. In particular, the actual loss is much higher than the theoretical value. This is mainly because Model 1 fails to model the actual operation of the coordinated PV inverter group. It is thus overly optimistic about the participation of the consumer-owned PV inverters in the optimization of the utility's VVC objective. By contrast, the theoretical loss with Model 2 is close to the actual loss. However, because this model is unable to use the reactive output from the PV inverters, its actual loss is higher than that with our proposed model. In particular, during the peak load period (19:00-22:00), the average power loss with Model 2 is 11% higher than the loss with our bi-level model, which demonstrates the benefits of incorporating the autonomous PV inverters in the utility's VVC optimization.

Table 3.3: Average Daily Active Power Loss

	Bi-level	Model 1	Model 2
Theoretical value P^*_{loss} (kW)	75.92	59.70	79.58
Actual value P_{loss} (kW)	78.50	92.82	81.82

3.5 Summary

This chapter proposes a bi-level optimization-based VVC framework for distribution networks with both conventional voltage control devices and smart residential PV inverters. The centralized upper-level optimization determines the setpoints for the OLTCs and CBs on an hourly-basis by solving a MISOCP optimization problem based on single-level reduction approach. This level takes advantages of the network information available to the ADMS and achieves system-wide optimal coordination among all control devices. The distributed lower-level optimization exploits the autonomous capability of the smart PV inverters by enabling them to adjust their outputs based on local voltage measurements and neighboring

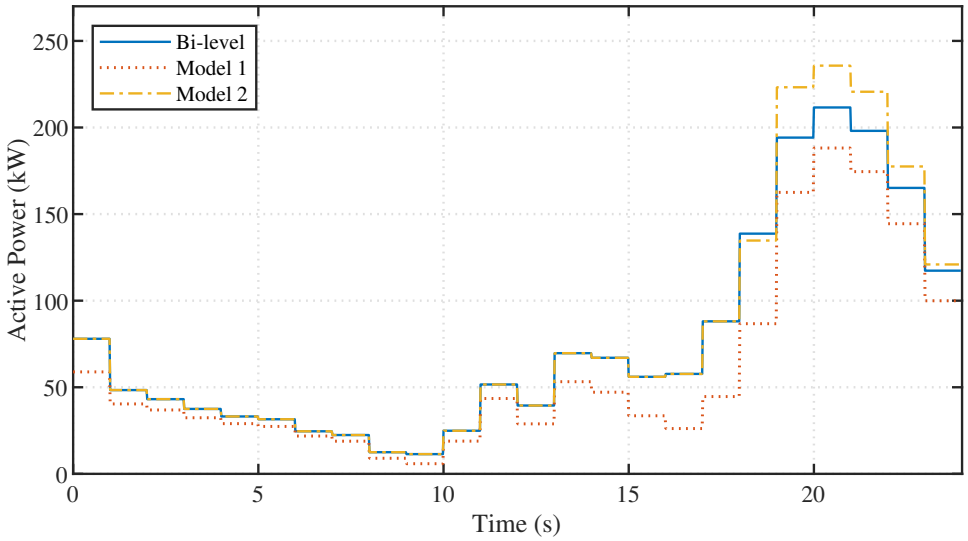

Figure 3.9: Theoretical daily network active power losses.

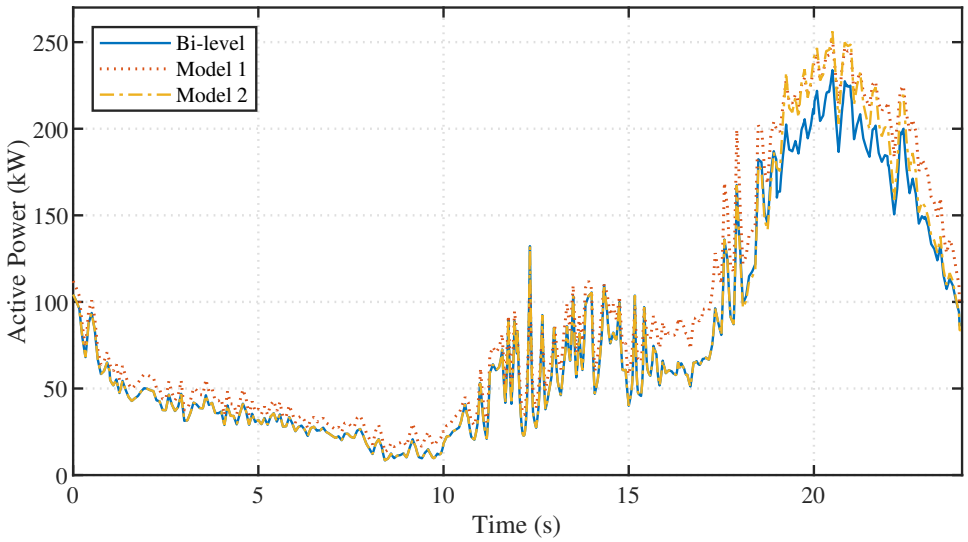

Figure 3.10: Actual daily network active power losses.

communication. It corrects the sudden voltage violations that occur during the upper-level dispatch periods and also achieves an optimal utilization of all the available inverter reactive power capacity. This VVC framework successfully captures the interactions between the mechanical devices and the autonomous inverters. Hence, it facilitates the coordination between these devices and fully exploits their capabilities for the voltage regulation. This framework represents an effective and flexible way for the distribution networks to accommodate autonomous PV inverters in the VVC architecture.

Chapter 4
CONCLUSION

This dissertation studies the coordinated voltage regulation for distribution networks with smart PV inverters. The adaptive coalition formation-based strategy developed in Chapter 2 enables the smart PV inverters to determine their scope of cooperation in response to the constantly-changing network operating condition. In this way, the potential conflict between voltage regulation and reactive power sharing can be effectively solved. The PV inverters within each coalition are thus able to eliminate real-time voltage violations while achieving an equal utilization ratio of their available reactive capacities. In Chapter 3, we extended the coordination scope into the whole distribution network, which includes both the autonomous smart PV inverters and the utility-dispatched mechanical devices. We applied the bi-level optimization model to capture the interactions between these two types of voltage regulation devices. Hence, the system operator would be able to schedule the mechanical devices while taking account of the voltage regulation actions of the smart PV inverter group. The corresponding two-timescale voltage regulation framework fully exploits the capabilities of the available devices to improve the dynamic voltage regulation performance and enhance the economical efficiency of the entire distribution network.

4.1 Key Results

The results showed that the adaptive coalition formation-based strategy proposed in Chapter 2 possesses the following properties:

- It provides an effective way for the smart PV inverters to achieve self-organization. Compared with traditional network partition strategy, the coalition formation scheme is more flexible and has better scalability.

- It coordinates the actions of the smart PV inverters within each coalition by emulating the iteration process of a distributed optimization algorithm, which guarantees the elimination of voltage violations and the convergence to the same utilization ratio.

- It is robust to communication latency and failure, and also generalizes well to networks with varying inverter quantities, locations and capacities.

In Chapter 3, we developed a two-timescale VVC framework based on the bi-level optimization model. The properties of this framework can be summarized as follows:

- It fully exploits the autonomous capability of the smart PV inverters to remove real-time voltage violations, which improves the dynamic voltage regulation performance and the robustness of the framework to the variability of load and PV active generation.

- It makes a sufficient use of the information available in the ADMS to optimally schedule the mechanical devices while considering the response of the smart PV inverters, which minimizes the network active power losses.

- It facilitates the coordination between different types of voltage regulation devices and thus effectively accommodates the autonomous and cooperative smart PV inverter group in the overall VVC architecture.

4.2 Suggestions for Future Research

On the basis of the research carried out in this dissertation, problems that merit further investigation include:

- Addressing the potential data privacy and cyber-attack issues. The cooperation of the smart PV inverters relies on the exchange of their state information among neighboring inverters. During the transmission process, either wired or wireless, these sensitive information are vulnerable to hackers [71]. The strategy proposed in Chapter 2 can

be improved with data encryption technology [72] or augmented privacy-preserving consensus algorithms [73, 74]. On the other hand, the cooperation of the smart PV inverters is conducted on the basis that all inverters are trustworthy and reliable. However, in the real-world implementation, cyber-attacks like false data injection and denial-of-service can happen [75]. Further study is needed to improve the robustness of the strategy proposed in Chapter 2 under various cyber-attacks.

- Handling the uncertainties in the PV active generation. The lower-level of the framework proposed in Chapter 3 organizes the smart PV inverters to eliminate the real-time voltage violations. However, the upper-level schedules the mechanical devices based on an hourly forecast of PV active power generation, where there can be forecast errors and uncertainties. Robust optimization algorithms [76, 77] can be employed to improve this upper-level.

- Applying data-driven algorithms for the optimal voltage regulation. Besides the PV active power forecast, errors and uncertainties also exist in the distribution network models. Data-driven optimal control strategies have been proven effective in dealing with such issues [78, 79, 80, 81, 82]. It can be expected that this will continue to be an exciting research field in the future.

- Designing the smart inverter reactive power compensation incentive mechanism. The small-scale PV inverters in the distribution networks are currently owned and operated by the power consumers. The utility does not have the authority to coordinate their control actions directly. Although the strategies we proposed in Chapter 2 and 3 support a flexible plug-and-play operation. The effectiveness of these strategies depends on the amount of PV inverters that are willing to participate in the voltage regulation. Incentive mechanisms which carefully balance the cost and benefit from both the utility and the consumer sides worth further exploration.

BIBLIOGRAPHY

[1] A. Von Meier. *Electric power systems*. Wiley Online Library, 2006.

[2] M. Karimi, H. Mokhlis, K. Naidu, S. Uddin, and A.H.A. Bakar. Photovoltaic penetration issues and impacts in distribution network–a review. *Renewable and Sustainable Energy Reviews*, 53:594–605, 2016.

[3] F. Katiraei and J. R. Agüero. Solar PV integration challenges. *IEEE Power and Energy Magazine*, 9(3):62–71, 2011.

[4] C. L. Masters. Voltage rise: the big issue when connecting embedded generation to long 11 kV overhead lines. *Power Engineering Journal*, 16(1):5–12, 2002.

[5] A. Woyte, V. Van Thong, R. Belmans., and J. Nijs. Voltage fluctuations on distribution level introduced by photovoltaic systems. *IEEE Transactions on Energy Conversion*, 21(1):202–209, 2006.

[6] R. Yan, B. Marais, and T. K. Saha. Impacts of residential photovoltaic power fluctuation on on-load tap changer operation and a solution using DSTATCOM. *Electric Power Systems Research*, 111:185–193, 2014.

[7] M. I. Hossain, R. Yan, and T. K. Saha. Investigation of the interaction between step voltage regulators and large-scale photovoltaic systems regarding voltage regulation and unbalance. *IET Renewable Power Generation*, 10(3):299–309, 2016.

[8] I. Kim and M. Begovic. On impact of randomly distributed PV systems on distribution networks. In *2016 49th Hawaii International Conference on System Sciences (HICSS)*, pages 2418–2425, 2016.

[9] A. Alrushoud and N. Lu. Impacts of PV capacity allocation methods on distribution planning studies. In *2020 IEEE/PES Transmission and Distribution Conference and Exposition (T D)*, pages 1–5, 2020.

[10] L. Wang, T. K. Saha, and R. Yan. Voltage regulation for distribution systems with uneven PV integration in different feeders. In *2017 IEEE Power Energy Society General Meeting*, pages 1–5, 2017.

[11] J. W. Smith, W. Sunderman, R. Dugan, and B. Seal. Smart inverter volt/var control functions for high penetration of PV on distribution systems. In *2011 IEEE/PES Power Systems Conference and Exposition*, pages 1–6, 2011.

[12] Y. Xu and J. M. Guerrero. Smart inverters for utility and industry applications. In *Proceedings of PCIM Europe 2015; International Exhibition and Conference for Power Electronics, Intelligent Motion, Renewable Energy and Energy Management*, pages 1–8, 2015.

[13] Y. Xue, M. Starke, J. Dong, M. Olama, T. Kuruganti, J. Taft, and M. Shankar. On a future for smart inverters with integrated system functions. In *2018 9th IEEE International Symposium on Power Electronics for Distributed Generation Systems (PEDG)*, pages 1–8, 2018.

[14] Common functions for smart inverters: 4th edition. EPRI, 2016.

[15] Solar Power Europe. Global market outlook for solar power 2020-2024, 2020.

[16] R. Tonkoski, D. Turcotte, and T. H. M. EL-Fouly. Impact of high PV penetration on voltage profiles in residential neighborhoods. *IEEE Transactions on Sustainable Energy*, 3(3):518–527, 2012.

[17] R. Yan and T. K. Saha. Investigation of voltage stability for residential customers due to high photovoltaic penetrations. *IEEE Transactions on Power Systems*, 27(2):651–662, 2012.

[18] IEEE standard for interconnection and interoperability of distributed energy resources with associated electric power systems interfaces. *IEEE Std 1547-2018 (Revision of IEEE Std 1547-2003)*, 2018.

[19] P. Jahangiri and D. C. Aliprantis. Distributed Volt/VAr control by PV inverters. *IEEE Transactions on Power Systems*, 28(3):3429–3439, 2013.

[20] A. Kulmala, S. Repo, and P. Järventausta. Coordinated voltage control in distribution networks including several distributed energy resources. *IEEE Transactions on Smart Grid*, 5(4):2010–2020, 2014.

[21] S. Magnússon, G. Qu, and N. Li. Distributed optimal voltage control with asynchronous and delayed communication. *IEEE Transactions on Smart Grid*, 11(4):3469–3482, 2020.

[22] G. Qu and N. Li. Optimal distributed feedback voltage control under limited reactive power. *IEEE Transactions on Power Systems*, 35(1):315–331, 2020.

[23] G. Mokhtari, A. Ghosh, G. Nourbakhsh, and G. Ledwich. Smart robust resources control in LV network to deal with voltage rise issue. *IEEE Transactions on Sustainable Energy*, 4(4):1043–1050, 2013.

[24] Y. Wang, K. T. Tan, X. Y. Peng, and P. L. So. Coordinated control of distributed energy-storage systems for voltage regulation in distribution networks. *IEEE Transactions on Power Delivery*, 31(3):1132–1141, 2016.

[25] M. Zeraati, M. E. Hamedani Golshan, and J. M. Guerrero. A consensus-based cooperative control of PEV battery and PV active power curtailment for voltage regulation in distribution networks. *IEEE Transactions on Smart Grid*, 10(1):670–680, 2019.

[26] M. Zeraati, M. E. H. Golshan, and J. M. Guerrero. Voltage quality improvement in low voltage distribution networks using reactive power capability of single-phase PV inverters. *IEEE Transactions on Smart Grid*, 10(5):5057–5065, 2019.

[27] G. Mokhtari, G. Nourbakhsh, and A. Ghosh. Smart coordination of energy storage units (ESUs) for voltage and loading management in distribution networks. *IEEE Transactions on Power Systems*, 28(4):4812–4820, 2013.

[28] Y. Wang, M. H. Syed, E. Guillo-Sansano, Y. Xu, and G. M. Burt. Inverter-based voltage control of distribution networks: A three-level coordinated method and power hardware-in-the-loop validation. *IEEE Transactions on Sustainable Energy*, 11(4):2380–2391, 2020.

[29] B. Horling and V. Lesser. A survey of multi-agent organizational paradigms. *Knowledge Engineering Review*, 19(4):281–316, 2004.

[30] V. C. Gungor and F. C. Lambert. A survey on communication networks for electric system automation. *Computer Networks*, 50(7):877–897, 2006.

[31] R. Olfati-Saber and R. M. Murray. Consensus problems in networks of agents with switching topology and time-delays. *IEEE Transactions on Automatic Control*, 49(9):1520–1533, 2004.

[32] D. Ye, M. Zhang, and D. Soetanto. Decentralized dispatch of distributed energy resources in smart grids via multi-agent coalition formation. *Journal of Parallel and Distributed Computing*, 83:30–43, 2015.

[33] F. Luo, Z. Y. Dong, G. Liang, J. Murata, and Z. Xu. A distributed electricity trading system in active distribution networks based on multi-agent coalition and blockchain. *IEEE Transactions on Power Systems*, 34(5):4097–4108, 2019.

[34] F. Ren, M. Zhang, D. Soetanto, and X. Su. Conceptual design of a multi-agent system for interconnected power systems restoration. *IEEE Transactions on Power Systems*, 27(2):732–740, 2012.

[35] B.A. Faiya, D. Athanasiadis, M. J. Chen, S. McArthur, I. Kockar, H. Lu, and F. de León. A self organizing multi agent system for distributed voltage regulation. *IEEE Transactions on Smart Grid*, 2021.

[36] P. Li, C. Zhang, Z. Wu, Y. Xu, M. Hu, and Z. Dong. Distributed adaptive robust voltage/var control with network partition in active distribution networks. *IEEE Transactions on Smart Grid*, 11(3):2245–2256, 2020.

[37] R. Olfati-Saber, J. A. Fax, and R. M. Murray. Consensus and cooperation in networked multi-agent systems. *Proceedings of the IEEE*, 95(1):215–233, 2007.

[38] C. Chang, M. Colombino, J. Corté, and E. Dall'Anese. Saddle-flow dynamics for distributed feedback-based optimization. *IEEE Control Systems Letters*, 3(4):948–953, 2019.

[39] Toronto and Region Conservation Authority (TRCA) and York University. Managing Volt/VAR in active distribution networks using distributed generation units and peer to peer communication. Toronto and Region Conservation Authority, 2018.

[40] G. Hug C. Wu and S. Kar. Smart inverter for voltage regulation: Physical and market implementation. *IEEE Transactions on Power Systems*, 33(6):6181–6192, 2018.

[41] M. Joyce. Advanced inverter functions to support high levels of distributed solar. National Renewable Energy Laboratory, 2015.

[42] B. Wei, Z. Qiu, and G. Deconinck. A mean-field voltage control approach for active distribution networks with uncertainties. *IEEE Transactions on Smart Grid*, 12(2):1455–1466, 2021.

[43] Pecan street Inc. Dataport. `https://dataport.pecanstreet.org/`, 2019. [Online].

[44] EnerNOC Open Data. `https://open-enernoc-data.s3.amazonaws.com/anon/index.html`. [Online].

[45] R. D. Zimmerman, C. E. Murillo-Sánchez, and R. J. Thomas. MATPOWER: Steady-state operations, planning, and analysis tools for power systems research and education. *IEEE Transactions on Power Systems*, 26(1):12–19, 2011.

[46] M. Farivar and S. H. Low. Branch flow model: Relaxations and convexification—part i. *IEEE Transactions on Power Systems*, 28(3):2554–2564, 2013.

[47] N. Li, G. Qu, and M. Dahleh. Real-time decentralized voltage control in distribution networks. In *2014 52nd Annual Allerton Conference on Communication, Control, and Computing (Allerton)*, pages 582–588, 2014.

[48] O. Gandhi, C. D. Rodríguez-Gallegos, N. B. Y. Gorla, M. Bieri, T. Reindl, and D. Srinivasan. Reactive power cost from PV inverters considering inverter lifetime assessment. *IEEE Transactions on Sustainable Energy*, 10(2):738–747, 2019.

[49] R. C. Dugan. Reference guide: The open distribution system simulator (OpenDSS). *Electric Power Research Institute, Inc*, 7:29, 2012.

[50] IEEE PES Distribution Systems Analysis Subcommittee. Radial test feeders. `https://site.ieee.org/pes-testfeeders/resources/`. [Online].

[51] T. Gönen. *Electric power distribution engineering*. CRC press, 2015.

[52] R. R. Jha, A. Dubey, C. Liu, and K. P. Schneider. Bi-level Volt-VAR optimization to coordinate smart inverters with voltage control devices. *IEEE Transactions on Power Systems*, 34(3):1801–1813, 2019.

[53] Q. Zhang, K. Dehghanpour, and Z. Wang. Distributed CVR in unbalanced distribution systems with PV penetration. *IEEE Transactions on Smart Grid*, 10(5):5308–5319, 2019.

[54] Y. Guo, Q. Wu, H. Gao, S. Huang, B. Zhou, and C. Li. Double-time-scale coordinated voltage control in active distribution networks based on MPC. *IEEE Transactions on Sustainable Energy*, 11(1):294–303, 2020.

[55] Y. Xu, Z. Y. Dong, R. Zhang, and D. J. Hill. Multi-timescale coordinated voltage/var control of high renewable-penetrated distribution systems. *IEEE Transactions on Power Systems*, 32(6):4398–4408, 2017.

[56] T. Ding, S. Liu, W. Yuan, Z. Bie, and B. Zeng. A two-stage robust reactive power optimization considering uncertain wind power integration in active distribution networks. *IEEE Transactions on Sustainable Energy*, 7(1):301–311, 2016.

[57] F. Dörfler, S. Bolognani, J. W. Simpson-Porco, and S. Grammatico. Distributed control and optimization for autonomous power grids. In *2019 18th European Control Conference (ECC)*, pages 2436–2453, 2019.

[58] C. Zhang, Y. Xu, Z. Dong, and J. Ravishankar. Three-stage robust inverter-based voltage/var control for distribution networks with high-level PV. *IEEE Transactions on Smart Grid*, 10(1):782–793, 2019.

[59] A. R. Malekpour, A. M. Annaswamy, and J. Shah. Hierarchical hybrid architecture for Volt/Var control of power distribution grids. *IEEE Transactions on Power Systems*, 35(2):854–863, 2020.

[60] R. R. Jha, A. Dubey, and K. P. Schneider. Conservation voltage reduction (CVR) via two-timescale control in unbalanced power distribution systems. *IET Smart Grid*, 3(6):801–813, 2020.

[61] H. S. Bidgoli and T. Van Cutsem. Combined local and centralized voltage control in active distribution networks. *IEEE Transactions on Power Systems*, 33(2):1374–1384, 2018.

[62] T. Hong, D. Zhao, Y. Zhang, B. Cui, and Y. Tian. Optimal voltage reference for droop-based DERs in distribution systems. *IEEE Transactions on Smart Grid*, 11(3):2357–2366, 2020.

[63] C. Zhang and Y. Xu. Hierarchically-coordinated Voltage/VAR control of distribution networks using PV inverters. *IEEE Transactions on Smart Grid*, 11(4):2942–2953, 2020.

[64] S. Bolognani, R. Carli, G. Cavraro, and S. Zampieri. On the need for communication for voltage regulation of power distribution grids. *IEEE Transactions on Control of Network Systems*, 6(3):1111–1123, 2019.

[65] S. Bolognani, R. Carli, G. Cavraro, and S. Zampieri. Distributed reactive power feedback control for voltage regulation and loss minimization. *IEEE Transactions on Automatic Control*, 60(4):966–981, 2015.

[66] S. Magnússon, G. Qu, C. Fischione, and N. Li. Voltage control using limited communication. *IEEE Transactions on Control of Network Systems*, 6(3):993–1003, 2019.

[67] D. Ranamuka, A. P. Agalgaonkar, and K. M. Muttaqi. Examining the interactions between DG units and voltage regulating devices for effective voltage control in distribution systems. *IEEE Transactions on Industry Applications*, 53(2):1485–1496, 2017.

[68] M. E. Baran and F. F. Wu. Network reconfiguration in distribution systems for loss reduction and load balancing. *IEEE Transactions on Power Delivery*, 4(2):1401–1407, 1989.

[69] A. Sinha, P. Malo, and K. Deb. A review on bilevel optimization: From classical to evolutionary approaches and applications. *IEEE Transactions on Evolutionary Computation*, 22(2):276–295, 2018.

[70] L. Ortmann, A. Prostejovsky, K. Heussen, and S. Bolognani. Fully distributed peer-to-peer optimal voltage control with minimal model requirements. *Electric Power Systems Research*, 189:106717, 2020.

[71] Y. Wang. Privacy-preserving average consensus via state decomposition. *IEEE Transactions on Automatic Control*, 64(11):4711–4716, 2019.

[72] K. Gai, M. Qiu, H. Zhao, and J. Xiong. Privacy-aware adaptive data encryption strategy of big data in cloud computing. In *2016 IEEE 3rd International Conference on Cyber Security and Cloud Computing (CSCloud)*, pages 273–278, 2016.

[73] H. Xu, y. Ni, z. Liu, and Z. Chen. Privacy-preserving leader-following consensus via node-augment mechanism. *IEEE Transactions on Circuits and Systems II: Express Briefs*, 68(6):2117–2121, 2021.

[74] X. Duan, J. He, P. Cheng, Y. Mo, and J. Chen. Privacy preserving maximum consensus. In *2015 54th IEEE Conference on Decision and Control (CDC)*, pages 4517–4522, 2015.

[75] Y. Liu, H. Xin, Z. Qu, and D. Gan. An attack-resilient cooperative control strategy of multiple distributed generators in distribution networks. *IEEE Transactions on Smart Grid*, 7(6):2923–2932, 2016.

[76] D. Bertsimas, E. Litvinov, X. A. Sun, J. Zhao, and T. Zheng. Adaptive robust optimization for the security constrained unit commitment problem. *IEEE Transactions on Power Systems*, 28(1):52–63, 2013.

[77] B. Zeng and L. Zhao. Solving two-stage robust optimization problems using a column-and-constraint generation method. *Operations Research Letters*, 41(5):457–461, 2013.

[78] Q. Yang, G. Wang, A. Sadeghi, G. B. Giannakis, and J. Sun. Two-timescale voltage control in distribution grids using deep reinforcement learning. *IEEE Transactions on Smart Grid*, 11(3):2313–2323, 2020.

[79] S. Wang, J. Duan, D. Shi, C. Xu, H. Li, R. Diao, and Z. Wang. A data-driven multi-agent autonomous voltage control framework using deep reinforcement learning. *IEEE Transactions on Power Systems*, 35(6):4644–4654, 2020.

[80] S. Wang, J. Duan, D. Shi, C. Xu, H. Li, R. Diao, and Z. Wang. Data-driven optimal voltage regulation using input convex neural networks. *Electric Power Systems Research*, 189:106741, 2020.

[81] D. Cao, J. Zhao, W. Hu, F. Ding, Q. Huang, Z. Chen, and F. Blaabjerg. Data-driven multi-agent deep reinforcement learning for distribution system decentralized voltage control with high penetration of PVs. *IEEE Transactions on Smart Grid*, pages 1–1, 2021.

[82] X. Lei, Z. Yang, J. Yu, J. Zhao, Q. Gao, and H. Yu. Data-driven optimal power flow: A physics-informed machine learning approach. *IEEE Transactions on Power Systems*, 36(1):346–354, 2021.

Appendix A

SUPPLEMENTARY MATERIAL TO CHAPTER 3

A.1 Nomenclatures

Sets and Indices

$\mathcal{E}$, ij	Set, index of all the network branches
$\mathcal{N}_{\mathcal{G}}$	Set of nodes with PV
$\mathcal{N}$, i	Set, index of all the network nodes
k	Index of the iteration cycles in the lower-level
t	Index of the dispatch periods in the upper-level

Variables

l_{ij}	Squared current magnitude on branch ij
n_{ij}^{T}	Tap position of the OLTC on branch ij
n_{i}^{C}	Number of the CB units at node i
P_{ij}, Q_{ij}	Active, reactive power flow on branch ij
q_{i}^{g}	Reactive power output of the PV at node i
v_{i}	Squared voltage magnitude at node i

Parameters

$\bar{l}_{ij}$	Upper limit for the squared current magnitude on branch ij
$\bar{n}_{ij}^T$	Maximum total tap change of the OLTC on branch ij over the dispatch horizon
$\bar{n}_i^C$	Maximum total change of the CB units at node i over the dispatch horizon
$\bar{q}_i^g$, $\underline{q}_i^g$	Upper, lower limit of the reactive power output of the PV at node i
$\bar{v}_i$, $\underline{v}_i$	Upper, lower limit for the squared voltage magnitude at node i
$\Delta\bar{n}_{ij}^T$	Maximum tap change of the OLTC on branch ij between two dispatch periods
$\Delta\bar{n}_i^C$	Maximum change of the CB units at node i between two dispatch periods
$\hat{p}_i^g$, p_i^g	Forecast, actual active power output of the PV at node i
$\hat{p}_i^l$, $\hat{q}_i^l$	Forecast active, reactive load at node i
N_{ij}^T	Total tap positions of the OLTC on branch ij
N_i^C	Total number of the CB units at node i
Q_i^C	Total capacity of the CB units at node i
r_{ij}, x_{ij}	Resistance, reactance of branch ij
s_i^g	Capacity of the PV inverter at node i

A.2 Proof of Objective Function (3.25)

The lower-level optimization model for equalizing the utilization ratios can be summarized as follows (the subscript t is omitted in this section):

$$\begin{aligned} \min_{\mathbf{q}^g} \quad & \sum_{i\in\mathcal{N}_\mathcal{G}} \frac{X_{li}}{2\bar{q}_i}(q_i^g)^2 \\ \text{s.t.} \quad & \underline{v} \le v_l^g \le \bar{v}, \\ & \underline{q}_i \le q_i^g \le \bar{q}_i,\ \forall i \in \mathcal{N}_\mathcal{G} \end{aligned} \tag{A.1}$$

where v_l^g is the local voltage of the leader inverter. The voltage constraint $\underline{v} \leq v_i \leq \bar{v}$, $\forall i \in \mathcal{N}_\mathcal{G}$ in (3.20) is replaced by $\underline{v} \leq v_l^g \leq \bar{v}$ here because the the utilization ratio of the inverter group is determined solely by this voltage. Assume problem (A.1) is feasible and the Slater condition is satisfied, i.e. there exist $\underline{q}_i < q_i^g < \bar{q}_i$, $\forall i \in \mathcal{N}_\mathcal{G}$ such that $\underline{v} < v_l^g < \bar{v}$, given the strong convexity of the cost function, this problem has a unique optimal solution.

To prove that this optimal solution promotes an equal utilization ratio in the PV inverter group, we first ignore the reactive power constraint and obtain the following Lagrangian function:

$$\mathcal{L}(q_i^g, \underline{\xi}, \bar{\xi}) = \sum_{i \in \mathcal{N}_\mathcal{G}} \frac{X_{li}}{2\bar{q}_i}(q_i^g)^2 + \underline{\xi}(\underline{v} - v_l^g) + \bar{\xi}(v_l^g - \bar{v}) \tag{A.2}$$

where $\underline{\xi}$ and $\bar{\xi}$ are the dual variables for the lower and upper voltage limit constraints. The derivative of $\mathcal{L}(q_i^g, \underline{\xi}, \bar{\xi})$ is:

$$\nabla_{q_i^g}\mathcal{L}(q_i^g, \underline{\xi}, \bar{\xi}) = \frac{X_{li}}{\bar{q}_i} q_i^g + (\bar{\xi} - \underline{\xi})\frac{\partial v_l^g}{\partial q_i^g} \tag{A.3}$$

where $\partial v_l^g / \partial q_i^g$ is the sensitivity of the leader inverter's local voltage to inverter i's reactive output. By approximating it as X_{li} [70] and setting $\nabla_{q_i^g}\mathcal{L}(q_i^g, \underline{\xi}, \bar{\xi}) = 0$, we obtain the critical point:

$$q_{i,\text{unc}}^g = \bar{q}_i(\underline{\xi} - \bar{\xi}). \tag{A.4}$$

This is the critical point when the reactive output is unconstrained. The solution to the constrained optimization problem (A.1) is obtained by projecting $\mathbf{q}_{\text{unc}}^g$ onto the set of feasible reactive output region. Due to the special structure of the objective function, this can be handled by projecting each $q_{i,\text{unc}}^g$, $\forall i \in \mathcal{N}_\mathcal{G}$ to its independent bounds $[\underline{q}_i, \bar{q}_i]$. Details of the proof can be found in [21]. Thus, we have the constrained optimizer:

$$q_{i,\text{opt}}^g = \left[\bar{q}_i(\underline{\xi} - \bar{\xi})\right]_{\underline{q}_i}^{\bar{q}_i}. \tag{A.5}$$

The utilization ratio of the inverter is:

$$u_i = \frac{q_{i,\text{opt}}^g}{\bar{q}_i} = \left[(\underline{\xi} - \bar{\xi})\right]_{-1}^{1}. \tag{A.6}$$

That is, a group of PV inverters that cooperate to solve the optimization problem (A.1) will converge on the same utilization ratio.

VITA

Yao Long received the B.Eng. degree in Electrical Engineering and Automation from Huazhong University of Science and Technology, Wuhan, China, in 2014. She obtained her M.Sc degree in Electrical Engineering from the University of Washington, Seattle, WA, USA, in 2016, where she is currently pursuing the Ph.D. degree. Her research interests include power system voltage regulation, distributed control and optimization, smart inverter and renewable generation.